

The physical mechanism for vortex merging

By C. CERRETELLI AND C. H. K. WILLIAMSON

Sibley School of Mechanical and Aerospace Engineering, Upson Hall, Cornell University, Ithaca,
NY 14853-7501, USA

(Received 11 April 2002 and in revised form 12 August 2002)

In this paper, we study the interaction of two co-rotating trailing vortices. It is well-known that vortices of like-sign ultimately merge to form a single vortex, and there has been much work on measuring and predicting the initial conditions for the onset of merger, especially concerning the critical vortex core radius. However, the physical mechanism causing this merger has received little attention. In this work, we directly measure the structure of the antisymmetric vorticity field that causes the co-rotating vortices to be pushed towards each other during merger. We discover that the form of the antisymmetric vorticity comprises two counter-rotating vortex pairs, whose induced velocity field readily pushes the two centroids together. The merging velocity computed from the antisymmetric vorticity field agrees closely with the merging velocity measured directly from the total (original) flow field.

The co-rotating vortex pair evolves through four distinct phases. The initial stage comprises a diffusive growth, which can be either viscous or turbulent. In either case, the number of turns that they rotate around one another until the vortices start to merge increases with Reynolds number (Re). If one observes the streamlines in a rotating reference frame (moving with the vortices), then one finds an inner and outer recirculating region of the flow bounded by a separatrix streamline. When the vortices grow large enough in the first stage, diffusion across the separatrix places vorticity into the outer recirculating region of the flow, and this leads to the generation of the antisymmetric vorticity, causing convective merger. This second (convective) stage corresponds to the motion of the vortex centroids towards each other, and is a process which is almost independent of viscosity. During the late part of this stage, the antisymmetric vorticity is diminished by a symmetrization process, and the final merging into one vorticity structure is achieved by a second diffusive stage. The fourth and ultimate phase is one where the merged vortex core grows by diffusion.

1. Introduction

The study of merging of co-rotating vortices has received much attention over the last few years. One of the reasons is linked to the renewed interest in the dynamics of coherent structures, which contain most of the kinetic energy of turbulent flows (Holmes, Lumley & Berkooz 1996). The merger of these structures (vortex pairing) plays a major role in the decay of two-dimensional turbulence and the growth of larger structures (see, for example, Couder 1983; McWilliams 1990; Jimenez, Moffatt & Vasco 1996; Clercx, Maassen & van Heijst 1999). As mentioned in the review paper by Hopfinger & van Heijst (1993), ‘this merger process is the predominant mechanism for the evolution of decaying two-dimensional turbulence, and has for this reason been studied extensively’. Vortex merger is important to three-dimensional turbulence (Vincent & Meneguzzi 1991) and mixing layers (Huerre & Rossi 1998). In order

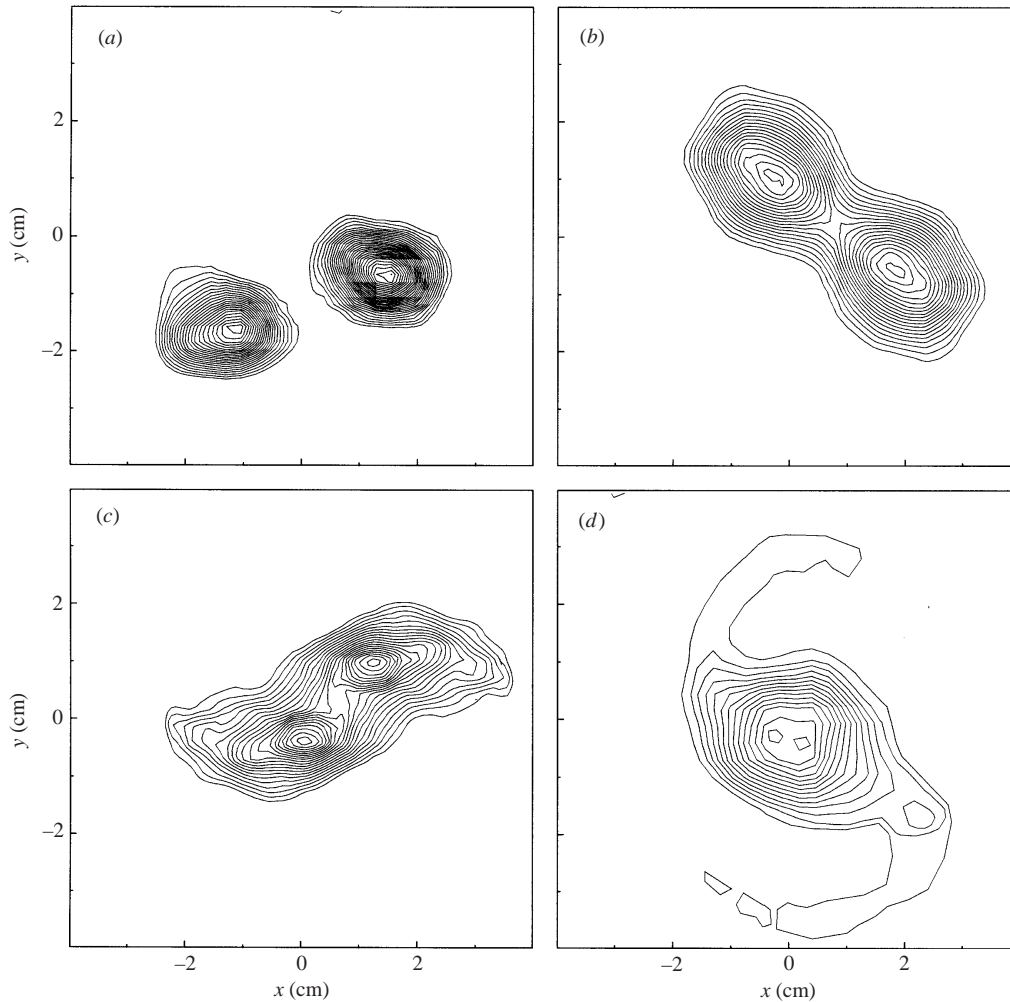


FIGURE 1. Vorticity fields during the merging process of two co-rotating vortices. In (a) and (b), the merging process is in the diffusive stage, while (c) and (d) show the convective merging stage. (a) $t = 2.1$ s; (b) $t = 13.3$ s; (c) $t = 19.6$ s; (d) $t = 30.8$ s. Vorticity contours are in steps of $\Delta\omega = 0.05 \text{ s}^{-1}$, with the lowest contour level being $\omega = 0.15 \text{ s}^{-1}$. Vorticity is counterclockwise.

to understand the behaviour of coherent structures, it is necessary to analyse and fully understand elementary vortex dynamics. A pair of co-rotating vortices of equal strength, which constitutes the object of the present study, is one of the most basic examples of such flows. In addition to its fundamental interest, an understanding of vortex merger has engineering applications. Co-rotating vortex pairs are found in the vortex system generated by aircraft wings, in flap-down configuration during take-off and landing. Such trailing vortex wakes, whose long lifetime constitutes a serious and known wake hazard, provide a limit to airport capabilities (Rossow 1977; Spalart 1998), and the process of merger can affect the efficiency of techniques to break up such wakes (Crouch 1997; Spalart 1998).

Essential features of vortex merger are illustrated in figure 1, showing the dynamics of vorticity from one of our experiments, where the two anticlockwise vortices are generated from the tips of two parallel rectangular wings pulled through a tank of

water. The vortices are initially approximately axisymmetric, and rotate around one another. The strain rate of each vortex leads to a slight elliptical deformation of each vortex, as they diffuse and grow in radius, in (a) and (b). When the vortices reach a critical size, two filaments are formed at the outer edges of the vortices, as shown in (c) and (d). At this point, the two vortices are significantly deformed, their vortex centres are pushed together, and they rapidly merge into a single structure, leaving some of the vorticity as a thin filament spiral around the merged vortex. The resulting combined vortex then diffuses outwards, growing in size, and becoming more axisymmetric (as mentioned in Melander, McWilliams & Zabusky 1987).

The importance of vortex merging was observed clearly in the studies of separating boundary layers by Freymuth (1966), in the investigations of mixing layers by Winant & Browand (1974), and in the high-Reynolds-number turbulent shear layers of Brown & Roshko (1974). Vortex pairing of neighbouring coherent vortices is a key phenomenon leading to growth of mixing layers as they travel downstream. From inviscid two-dimensional computations, Christiansen & Zabusky (1973) observed vortex merging from like-signed vortices that were initially arranged in two vortex rows in the form of a Kármán vortex street.

A body of work has addressed the question of a critical core size above which merging of co-rotating vortices takes place. Much of the early work comes from computations. Using vortex methods, Roberts & Christiansen (1972) found that merging of uniform-vorticity patches ensued for certain ratios ($a/b > 0.29$) between the vortex core radius (a) and the vortex separation (b), while Rossow (1977) computed $a/b > 0.26$ – 0.30 . Contour dynamics of uniform-vorticity patches has been employed effectively by Zabusky, Hughes & Roberts (1979), Saffman & Szeto (1980), Overman & Zabusky (1982) and Dritschel (1985, 1986). One of the main results coming from these studies is that one can compute steady configurations of non-circular co-rotating vortex patches, although if the (equivalent) core size becomes too large (typically if $a/b > 0.32$), no equilibrium solutions are found to exist. Overman & Zabusky analysed the behaviour of perturbed initial configurations for $a/b > 0.32$, demonstrating that co-rotating vortices rapidly deform, generating filaments and ultimately merging into a single structure. Dritschel found that vortex configurations for $a/b > 0.32$ were unstable. In essence, it appears that below a certain core size, stable vortex patch configurations exist, whereas above such a core size, the vortices are unstable, they deform, filaments are generated, followed by the process of merger.

More recently, attention has been focused on co-rotating vortices which have distributed (non-uniform) vorticity, since the critical core size is found to be dependent on such distributions. Meunier *et al.* (2002) have deduced a new merging criterion, by introducing a characteristic core size $a_\omega = \sqrt{J}/\Gamma$, where J is the second moment of vorticity for a vortex of circulation Γ . In both theory and experiments, this parameter has a critical value for merging which varies much less than conventional measures of core size, when used for a variety of vorticity distributions. Typical values for core size are $a_\omega \approx 0.24$. Further studies of a family of distributed co-rotating vortices by Le Dizes & Verga (2002), suggest that two-vortex systems relax to a unique state which corresponds to the two-vortex system with Gaussian profiles.

Interestingly, there are far fewer experimental measurements of the evolution of core size and merging for co-rotating vortices. The first confirmation of a critical core size in an experiment is that of Griffiths & Hopfinger (1987), which is also discussed in Hopfinger & van Heijst (1993), who found $a/b > 0.30$ for merging, in a study of cyclonic and anticyclonic vortices in a rotating flow. Recently, Meunier & Leweke (2001) also find the critical core size of around $a/b = 0.29$, using the definition of

core size (a) as the radius of maximum azimuthal velocity. They also discover in this paper (and comprehensively described in Meunier & Leweke 2002), a new cooperative elliptic instability for Reynolds numbers ($Re = \Gamma/\nu$, where ν is the kinematic viscosity) in excess of 2000, where the co-rotating vortices are three-dimensionally unstable, and where there is a distinct phase relationship for the instabilities in each vortex. They find an excellent agreement between the experiments, theory and computations, for the spatial structure, wavelength and growth rates of this instability, in Meunier & Leweke (2002), and in Leweke *et al.* (2001).

Despite the large number of papers which study the initial conditions for vortex merging, the physical mechanism of merging is not so well studied. However, important steps forward in our understanding were made by Melander *et al.* (1987) and by Melander, Zabusky & McWilliams (1988) in two key papers. Melander *et al.* (1987) study the axisymmetrization of an ellipse of uniform vorticity, employing a co-rotating reference frame, as used also by Dritschel (1985). They find that filaments are formed by fluid which is initially placed in a region they describe as a ‘ghost vortex’, outside the vortex core region. Such vorticity is advected away from the vortex cores by this ‘ghost vortex’ outer flow, which has a sense of rotation opposite to that of the primary vortices (a consequence of the co-rotating streamfunction). The formation of asymmetric filaments breaks the elliptical symmetry. This process leads to what they define as their ‘axisymmetrization principle’, whereby elliptical-shaped vorticity contours are oriented at some angle with respect to the approximately elliptic streamlines. There is a net effect to reduce the aspect ratio of the elliptic vortex patch, and we thus have ‘axisymmetrization’ as an inviscid mechanism acting on a circulation (non-viscous) timescale. In their second paper, Melander *et al.* (1988), who were concerned with the merging of two co-rotating vortices, employ a ‘moment model’, where they deduce equations for the centroid positions, for the aspect ratio of the two vortices, and for their orientations. They view merging as the same mechanism that they describe (in the 1987 paper) for the axisymmetrization of an elliptic vortex patch, and suggest that ‘merger is an inviscid axisymmetrization process’, whereby the aspect ratio of the two vortex system is reduced. In essence, they propose that it is the tilting of the co-rotating streamline pattern relative to the vorticity contour pattern which gives rise to a reduction of the distance between the two co-rotating vortices.

Melander *et al.* (1988) recognize two possible states in merger; namely, the ‘viscous metastable state’ whose lifetime is governed by the dissipation timescale, and the ‘convective merger stage’, where vortices merge on a vortex circulation timescale. Support for these stages of merger has come recently from the extensive experiments of Meunier & Leweke (2001, 2002) who define three stages of merger, where they consider the third stage as the diffusion of the merged vortex.

A model of vortex merging has also been constructed by Meunier (2001), who considers the rate at which vorticity is advected out of the vortex cores and into the filaments. This process increases the angular momentum of part of the flow (J increases), and thus, by conservation of angular momentum, the cores correspondingly must approach each other (so that J decreases). This model is quite consistent with our description of merging in the present work.

Our approach to understanding the physical mechanism of merging here is to study the process by which antisymmetric circulation is generated, and by which vortex filaments are produced. In the present case, since the development of antisymmetric vorticity is the key to understand merger, we decompose the whole vorticity field into symmetric and antisymmetric components, and thus, in contrast to earlier studies,

we may qualitatively and quantitatively measure the induced velocity field from the antisymmetric vorticity, which readily pushes the two vortices together. Our experimental approach is to generate co-rotating wing-tip vortices. Co-rotating wing wake vortices have been studied by Devenport, Vogel & Zsoldos (1999), and by Chen, Jacob & Savas (1999). Wing wakes were also used in the early study by Brandt & Iversen (1977), who estimated, from flow visualization, the distance travelled downstream by vortices before they merge. Devenport *et al.* studied the complex turbulence found in such vortices (formed behind separate neighbouring wings), and deduced that the merging process pushes turbulence, originally formed in the wake of the wing spans, into the merged vortex core. Chen *et al.* found that vortex merging from a flapped wing occurs after about 0.8 orbit periods, independent of the Reynolds number.

Following a description of the experimental methods in the next section, we shall present the dynamics of vortex merger as a sequence of four phases in §3. In §4, we investigate the physical parameters and the non-dimensional groups, which govern the different phases of vortex merger, in the case of both laminar and turbulent diffusion. In §5, we show the evolution of the flow streamlines in a reference frame which rotates with the vortex pair, demonstrating how antisymmetric vorticity is generated. The structure of the antisymmetric vorticity, and its induced velocity field, which pushes the vortices towards each other, are then analysed in detail. Antisymmetric vorticity is generated at the expense of symmetric vorticity, but at the end of the merging process, the flow field modifies this distribution, returning most of the antisymmetric vorticity to a symmetric configuration. We show that the final merging of the two vortices into one structure is achieved by diffusion. The conclusions are presented in §6.

2. Experimental methods

2.1. Experimental arrangement

The co-rotating vortex flow was studied in a computer-controlled XY towing tank (measuring 6.2 m long \times 1.0 m wide \times 0.6 m deep), and the general arrangement of the experiment is shown schematically in figure 2. The vortices were generated in water by two vertical, rectangular-planform wings of 0.038 m chord, and 0.266 m (submerged) span. The airfoil section is a circular arc of 1.5 mm thickness and 0.05 camber ratio, which is set typically to an angle of attack of 6° . The carriage is driven via a continuous cable and pulley system, powered by a DC Servomotor system, at speeds from 1 to 15 cm s⁻¹. The resulting Reynolds numbers (based on the chord) were in the range $Re = 400\text{--}5700$.

Quantitative measurements of velocity fields were obtained by digital particle image velocimetry (DPIV), using 14-micron silver-coated glass spheres to seed the flow. These particles were illuminated by a laser sheet, of 5 mm thickness, from a 5 W continuous argon ion laser. Images of the particles were captured using a high-resolution CCD Kodak Megaplug (1008 \times 1018 pixels) camera, and transferred in real time to a PC. The image acquisition was controlled by an external timing circuitry that was triggered when the leading edge of the airfoils entered the laser sheet. Although the image rate could be on average 30 Hz, we could arrange for pairs of images, for determining the velocity, to have a time separation of much less than 33 ms when needed. Pairs of images were analysed using cross-correlation of sub-images described by Adrian (1991), and implemented digitally in the manner described by Willert & Gharib (1991) and Westerweel (1993). Further details of our implementation of the DPIV technique are described in Leweke & Williamson (1998).

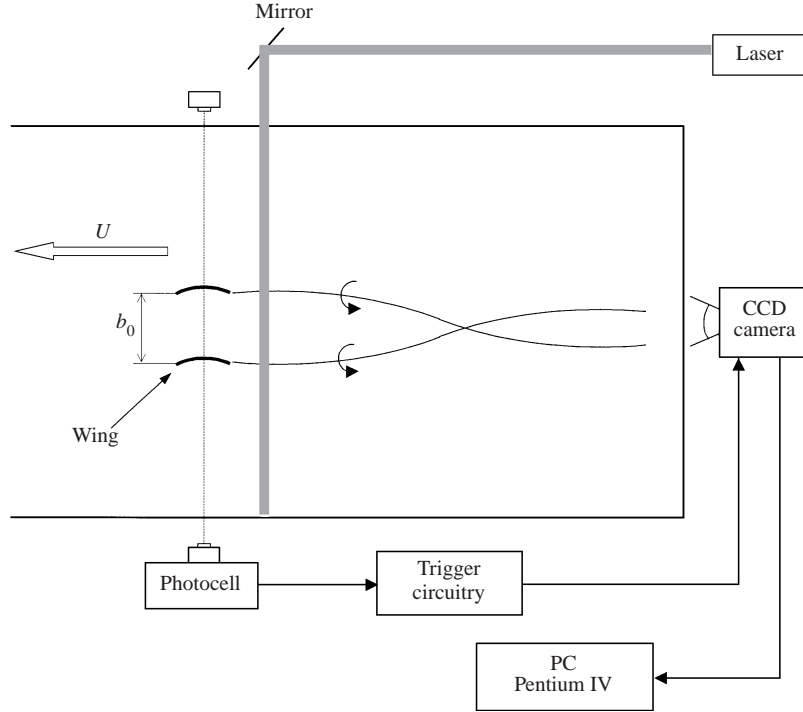


FIGURE 2. Schematic layout of the facility (looking vertically downwards) comprising the computer-controlled XY towing tank. A pair of vertical wings is towed through the fluid and generates two like-sign trailing vortices. The DPIV system utilizes the CCD camera, computer and argon-ion laser light sheet.

The coordinate system is as follows: the z -axis is in the downstream (towing) direction, measured from the trailing edge of the wing; the y -axis is vertical, while the x -axis is perpendicular to the towing direction and horizontal. In this work, we shall use the transformation $z = Ut$ to relate the downstream distance (z) to time (t), using the carriage velocity U .

2.2. Basic flow parameters and their determination

A co-rotating vortex pair is characterized by the following parameters, and shown diagrammatically in figure 3: the circulation of each vortex (Γ); the angle between the two vortices (θ); the separation between the vorticity maxima of the two vortices (b); and their core radius (a). In this section we will describe briefly how we determine these quantities. The circulation is computed from a contour line integral of the velocity around each vortex. The uncertainty associated with the measurement of the circulation is lower than if we integrate the vorticity within the vortex area. We estimate that the uncertainty is typically $\delta\Gamma/\Gamma \approx \pm 2\%$ for each vortex. We define the Reynolds number based on vortex strength $Re = \Gamma/\nu$, where ν is the kinematic viscosity of the flow.

In order to reduce irregularities in precisely determining the peak-vorticity location of a vortex, this location is taken as the centre of an area bounded by the contour line that is 80% of the peak vorticity value. Previous methods to find the vortex core radius, in the case of a two-dimensional patch of uniform vorticity in inviscid flow, whose shape may be non-circular, involve the use of an equivalent radius of the area

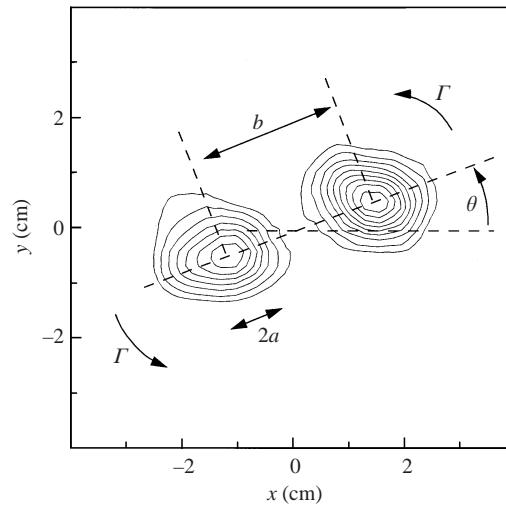


FIGURE 3. Definition of the parameters characterizing the vortex pair, for a typical experimental vorticity field. The principal parameters are the core radius (a), vortex separation between locations of peak vorticity (b), orientation of the co-rotating pair (θ), kinematic viscosity (ν) and vortex circulation (Γ). Vorticity is counterclockwise.

(A) of the patch, such that $a_{EQ} = \sqrt{A/\pi}$ (Saffman & Szeto 1980; Overman & Zabusky 1982). In the case of a real viscous flow, for example a counter-rotating vortex pair, the core radius has been measured from the best fit between the experimental velocity field and the velocity field generated by a pair of Lamb–Oseen vortices of Gaussian vorticity distribution (Lewke & Williamson 1998). For a co-rotating vortex pair, Meunier & Lewke (2001), and also the present results, show that the process of merging and vortex deformation make the match between a Gaussian vortex and the real vortex rather less accurate. Here we shall take the core radius (a) as the radius at which the azimuthal component of the velocity is a maximum. We analyse the mean azimuthal velocity outside the zone directly between the two vortices, employing a semi-circular region whose base is orthogonal to the line joining the two centres. Before merging, when we have two distinct vortices, the characteristic core size $a(t)$, defined in this way, is taken as the average of the core radii of the two vortices. After merger, the core size $a(t)$ defined by these means, naturally becomes the core radius of the merged vortex. During the merging process, the same method is employed to measure core radius (and we plot these data also), although its physical meaning is not as evident as the measured radius before and after the convective stage.

It should be mentioned here that we consider the velocity and vorticity fields, responsible for the physical merging process, as being principally two-dimensional, in that the flow field in the cross-sectional plane (normal to the towing direction) principally governs the vorticity dynamics. In the experimental arrangement, the co-rotating vortices spiral around one another, although the pitch wavelength is close to 200 cm, while the intervortex spacing is typically 3 cm, yielding a flow field closely approximating a two-dimensional flow. We should also mention that, based on the tip vortex measurement of Devenport *et al.* (1999), we may expect a small axial velocity within the cores of the vortices of less than 5% of the towing speed of the wings.

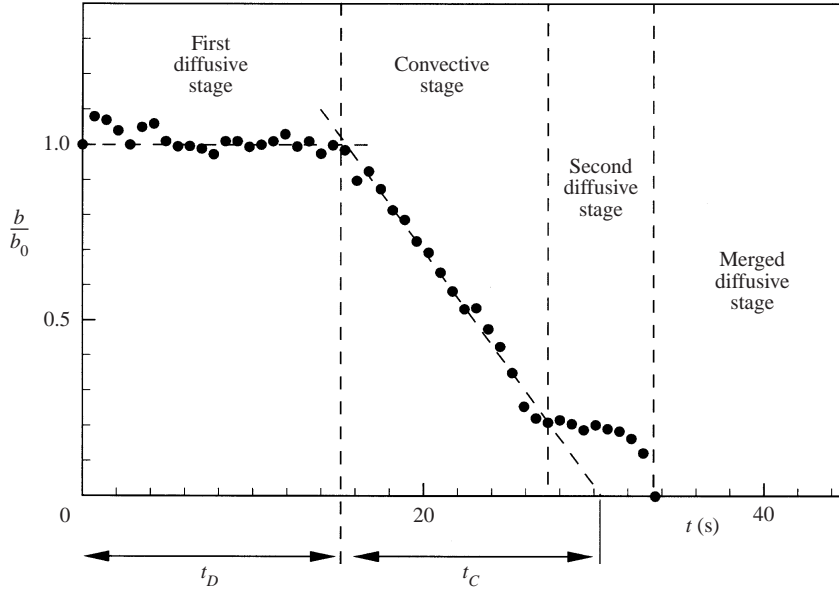


FIGURE 4. Evolution of the normalized vortex separation (b/b_0) versus time. From this curve it is possible to distinguish four distinct stages in the merging process ($Re = 530$).

3. Vortex merger as a four-stage process

The principal dynamics of the vortices during the process of merging are illustrated by the sequence of vorticity contour plots that were shown earlier in figure 1. As put forward in the theoretical work of Melander *et al.* (1988), and further defined in the experimental studies of Meunier & Leweke (2001, 2002), the dynamics of co-rotating vortices can be subdivided into three principal stages, namely the viscous and convective phases, followed ultimately by the diffusion of the merged vortex. These stages can perhaps best be defined in the present work with reference to the plot of vortex separation $b(t)$, shown in figure 4. In our case, we introduce a second diffusive stage at the end of merging, in essence defining four phases for the dynamics of co-rotating vortices, all of which will now be briefly outlined.

In the ‘first diffusive stage’, the vortices rotate around one another, while the vortex separation $b(t)$ remains essentially constant. In this stage, the angle between the vortices, $\theta(t)$, as shown in figure 5(a), increases linearly, since the angular velocity of the vortex pair is constant (and roughly equal to that found for two point vortices of the same circulation, Γ_0). It should be mentioned that a reasonable value of angular velocity of the co-rotating vortex system was evaluated by measuring the angular velocity of the vortex centres (or locations of peak vorticity). However, during the final stages of the merger, the peaks are close together and might lead to a small overestimation of the angular velocity of the outer regions of the merging vorticity distribution. The diffusive growth of the vortices, as shown in figure 5(b), is well represented by the spread of Lamb–Oseen vortices, giving the core radius $a(t)$ as

$$a^2 = a_0^2 + \text{constant} \times (vt). \quad (3.1)$$

The ‘convective stage’ really represents the heart of the vortex merging process. The vortices become markedly deformed, and vortex filaments are generated at the extremities of the pair. It will later be seen how this asymmetric deformation of each

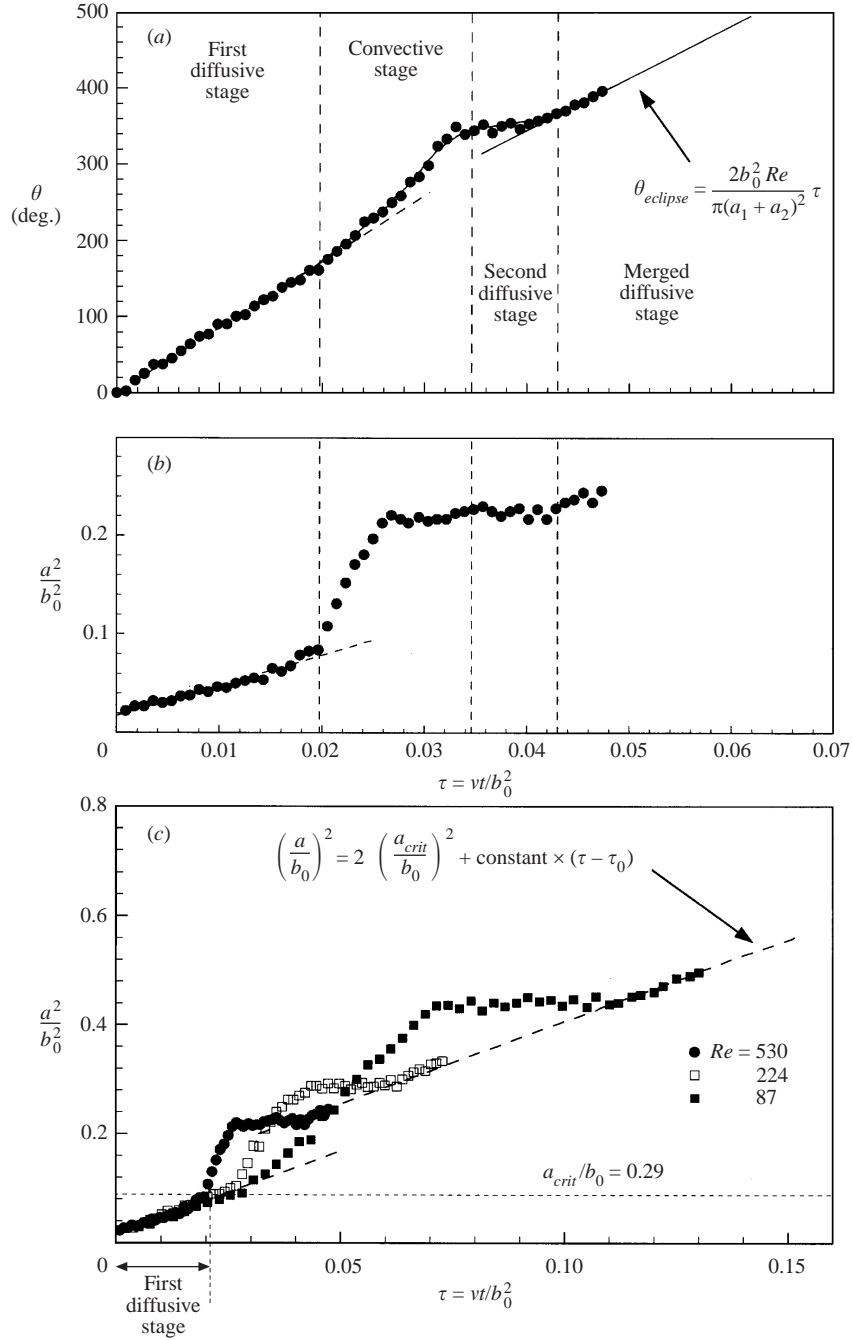


FIGURE 5. Evolution of the pair orientation (θ) and the core radius during the four stages of merging. In (a) and (b), we use the same timescale for this experiment at $Re = 530$. In (c), we compare the development of core radius $a(t)$ for different Re .

vortex is responsible for the rapid reduction in vortex separation $b(t)$, which in our case is approximately linear (as seen in figure 4, over the period of time labelled as t_C). The initiation of this stage in figure 4 can be defined well by the intersection of the line representing the diffusive regime when $b = \text{constant}$, with the linearly decreasing

line for the convective merging phase. The period of time spent in the first stage is defined as the diffusive time (t_D), and we shall define here the convective time (t_C) as the time it takes from the start of this convective stage until the point where an extrapolation of the linearly decreasing line $b(t)$ passes through the x -axis.

The ‘second diffusive stage’ represents a small regime where our measure of the vortex separation $b(t)$ ultimately reaches zero, at which point we define the vortices as ‘fully merged’. In this stage, the induced velocity, which is pushing the vortex centres together, is very small, and is not sufficient to cause the reduction of $b(t)$ to zero. The reduction of separation $b(t)$ is an apparent effect which is due to the method of measuring $b(t)$, which finds the ‘vortex centres’ (locations of peak vorticity). In essence, as described in §5, the vortices remain displaced by roughly $0.2b_0$, while vortex diffusion reduces the distance between vorticity maxima.

After the ‘fully merged’ condition is reached, the fourth phase of vortex dynamics is initiated, namely the ‘merged diffusive stage’, where the merged vortex, having an initially elliptical shape, gradually becomes more axisymmetric (although we do not study this ‘axisymmetrization phase’, described by Melander *et al.* 1987, in the present work), and diffuses at the rate of a single large vortex. The merged elliptical vortex appears to rotate with an angular velocity in reasonable agreement with the rotation of a Kirchhoff ellipse (an elliptic patch of uniform vorticity) of circulation $2\Gamma_0$, and semi-axes a_1 and a_2 (here we have $a_1/b_0 = 0.63$, and $a_2/b_0 = 0.94$, for the merged vortex, taking these measurements from the outer contours of the vortex):

$$\dot{\theta} = 2\Gamma_0/\pi(a_1 + a_2)^2 \quad (3.2)$$

which is plotted as the line in figure 5(a). The angular velocity of the elliptic vortex ($\dot{\theta}_E$) is approximately related to the initial angular velocity of the vortex pair ($\dot{\theta}_P$), by the simple expression

$$\dot{\theta}_E/\dot{\theta}_P = 2b_0^2/(a_1 + a_2)^2 \quad (3.3)$$

so that the ratio between velocities from (3.3) in our case is 0.81. For large Reynolds numbers, one can predict that the ratio of angular velocities will approach 2.8.

4. Laminar and turbulent vortex merger

In this section, we briefly study the timescales for the diffusive (t_D) and the convective (t_C) stages for the dynamics of co-rotating vortices. At a certain Reynolds number (which in this case is $Re \approx 800$), the vortex formation process of a wing-tip vortex renders the vortex turbulent, and this affects the timescales of the vortex merging. In their experimental study Meunier & Leweke (2001, 2002) find that the onset of elliptical (short-wave) instability in the vortices markedly affects the merging dynamics, accelerating merger relative to laminar vortices at comparable Reynolds numbers. The dynamics of turbulent vortices, in this study, are presented after a discussion on laminar vortex merging, which follows below.

4.1. Laminar vortex merging

In the present experiments, the initial vortex core size is approximately independent of Reynolds number, and is given by

$$\left(\frac{a_0}{b_0}\right) = 0.125 \pm 0.007. \quad (4.1)$$

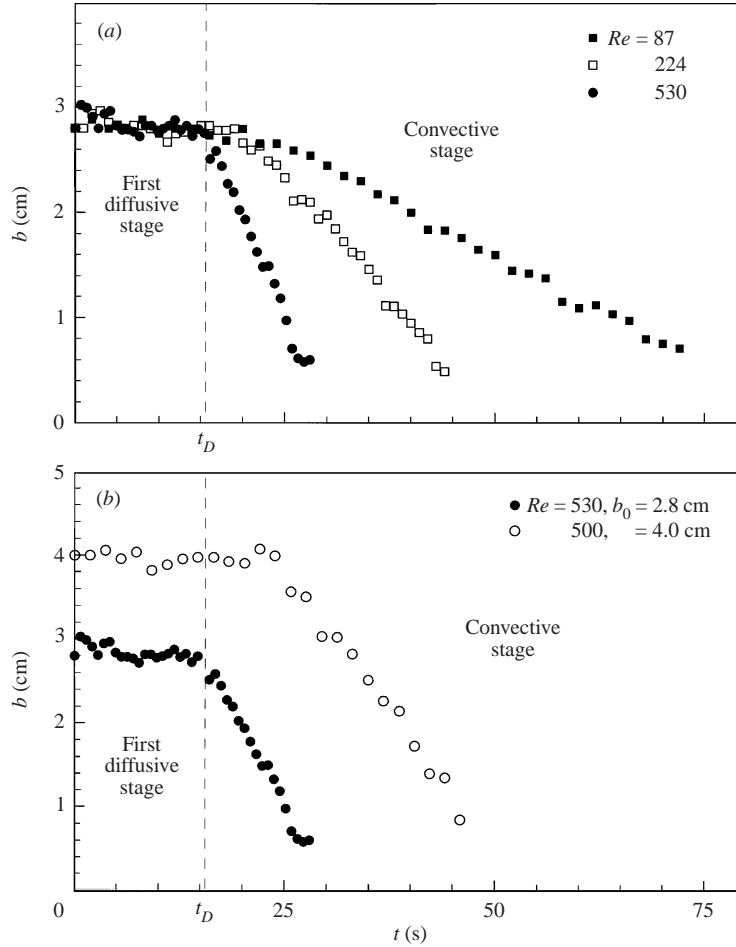


FIGURE 6. Evolution of the vortex separation distance as a function of time. In (a), we vary the Reynolds number, and in (b) these are two different initial vortex separations (different b_0).

We also find that the convective stage begins at a critical core size, given by

$$\left(\frac{a_{crit}}{b_0}\right) = 0.290 \pm 0.01. \quad (4.2)$$

The duration of the diffusive stage in these experiments is thus the time it takes for the vortex cores to grow from the initial size ($a = 0.125b_0$) to the critical size ($a = 0.29b_0$). In this study, the diffusive period (t_D) is reasonably independent of Re , as suggested by the results of figures 5 and 6. The critical core size is comparable with those values, for laminar vortices, found in Griffiths & Hopfinger (1987), who measured $a_{crit} \approx 0.30b_0$, and Meunier & Leweke (2001), who find $a_{crit} \approx 0.29b_0$.

The core radius growth $a(t)$ is dependent on the viscosity, and one expects it to roughly follow the diffusive growth of a viscous vortex:

$$a(t) = c\sqrt{v(t + t_0)} \quad (4.3)$$

(where t_0 is the (virtual) time it takes to reach an initial core size a_0 if we start with point vortices). Experimentally we find the value $c = 1.9 \pm 0.05$, which can

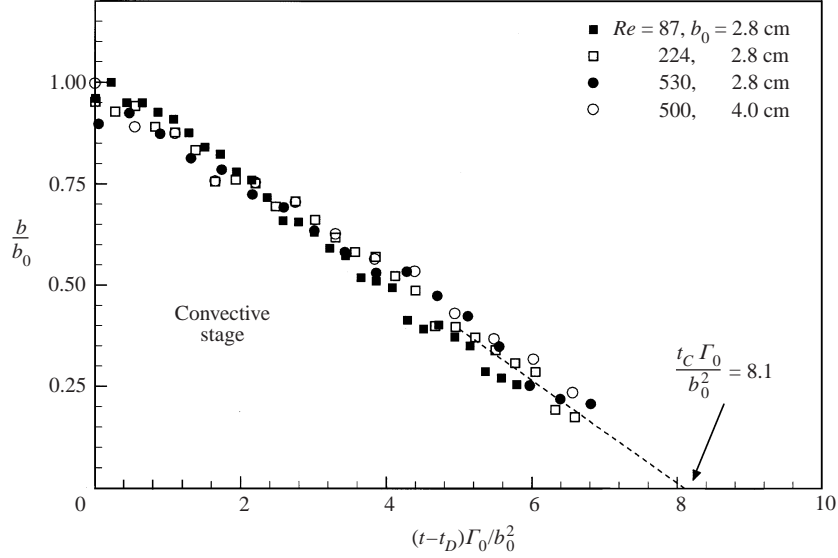


FIGURE 7. Vortex separation distance (b/b_0) as a function of the non-dimensional time $(t-t_D)\Gamma_0/b_0^2$ during the convective stage. The curves for different Reynolds numbers and initial separation distances (shown in figure 6) collapse very well onto a single line with this normalized timescale.

be compared with the theoretical value of $c = 2.24$ for Lamb–Oseen vortices. The duration of the diffusive stage is thus given by

$$t_D = \frac{1}{c^2\nu}(a_{crit}^2 - a_0^2). \quad (4.4)$$

The diffusive time (t_D) for laminar vortices in these experiments is therefore dependent on viscosity (ν) but not dependent on the vortex strength (Γ), although with stronger vortices (or higher Reynolds numbers), one expects that they will rotate around one another a greater number of turns by the end of this stage. On the other hand, in the convective stage, we expect that vortex strength will directly affect the duration of this stage (t_C), as we find below.

In the convective stage, we might expect the time taken for the vortex deformations, and for the subsequent pushing together of the two vortex centres, to be governed principally by the strength of the vortices (Γ_0) and the initial vortex spacing (b_0), and we might expect that this time (t_C) will be almost independent of the viscosity (ν). We can see in figure 6(a) that the vortex separation $b(t)$ decreases more rapidly in the case of the higher vortex strength Γ_0 (higher Reynolds number), and thus the convective period (t_C) is smaller. We can also see that if the initial spacing b_0 is larger, as in figure 6(b), then the convective period t_C will naturally be larger. Dimensionally, we expect that the convective period will scale as $t_C \sim b_0^2/\Gamma_0$, and so we introduce the timescale $(t-t_D)\Gamma_0/b_0^2$ in figure 7, and find a good collapse of all the vortex separation data $b(t)$ of figure 6 onto a single line. An extrapolation of all these data passes through the x -axis ($b = 0$), marking the end of what we define here as the convective period t_C , and giving the following value for this time period:

$$t_C = 8.1 \left(\frac{b_0^2}{\Gamma_0} \right). \quad (4.5)$$

The value of $t_C\Gamma_0/b_0^2$ can also be computed from the original data of previous experimental investigations (Griffiths & Hopfinger 1987; Meunier & Leweke 2001),

	Re	$t_C \Gamma_0 / b_0^2$
Present data	87	7.7
	224	8.2
	530	8.3
Meunier & Leweke (2001)	742	7.9
	1506	8.1
Griffiths & Hopfinger (1987)	740	8.1–9.7
	900	8.9

TABLE 1. The normalized convective time ($t_C \Gamma_0 / b_0^2$) for merging of laminar vortices computed from the original data of previous studies.

where one finds $t_C \Gamma_0 / b_0^2 \approx 7.9$ – 8.9 , for laminar vortices, as tabulated in table 1, in reasonable agreement with the present data. (There is some indication, within each set of data, that the time for the convective merger stage does increase very slightly with Re . This corresponds with the idea that the diffusion promotes the generation of antisymmetric vorticity during the convective stage, and therefore accelerates the motion of the vortices towards each other. However, such dependence on Re is rather weak, even at these low Re .) We can define a total merging time for laminar vortices as the time it takes for the vortices to ‘convectively merge’ from their initial formation:

$$t_m = t_D + t_C, \quad (4.6)$$

and using equations (4.4) and (4.5) we have

$$t_m = \frac{1}{c^2 \nu} (a_{crit}^2 - a_0^2) + 8.1 \frac{b_0^2}{\Gamma_0}. \quad (4.7)$$

We may normalize the merging time by the period $T = 2\pi^2 b_0^2 / \Gamma_0$, for which point vortices of the same initial strength (Γ_0) and spacing (b_0) would make one complete revolution around each other. The resulting normalized time (t_m^*) is approximately the number of turns until complete merger (N):

$$N \sim \frac{t_m}{T}. \quad (4.8)$$

Using equation (4.7), the normalized time for merging t_m^* is

$$t_m^* = \frac{Re}{2\pi^2 c^2} \left[\left(\frac{a_{crit}}{b_0} \right)^2 - \left(\frac{a_0}{b_0} \right)^2 \right] + 0.41. \quad (4.9)$$

One can see that if $(a_0/b_0) \approx \text{constant}$ for a set of experiments, then we have the simple result (as similarly deduced by Meunier *et al.* 2002):

$$t_m^* = c_1 Re + c_2, \quad (4.10)$$

where, in our case, $c_1 = 0.0011$ and $c_2 = 0.41$. We plot the variation of t_m^* with Re in figure 8, exhibiting a linear variation as one might expect. By also computing t_m^* from the data of Meunier & Leweke (2001), we find a similar line to our data, but with a smaller gradient because their initial core size is larger ($a_0/b_0 = 0.19$), and a similar intercept on the y -axis because their convective time is close to ours ($t_C \approx 0.39$). The plot also shows the maximum merging time (when $a_0/b_0 = 0$) and minimum t_m^* (when $a_0/b_0 = 0.29$), and so gives the approximate range of merging times that one might expect.

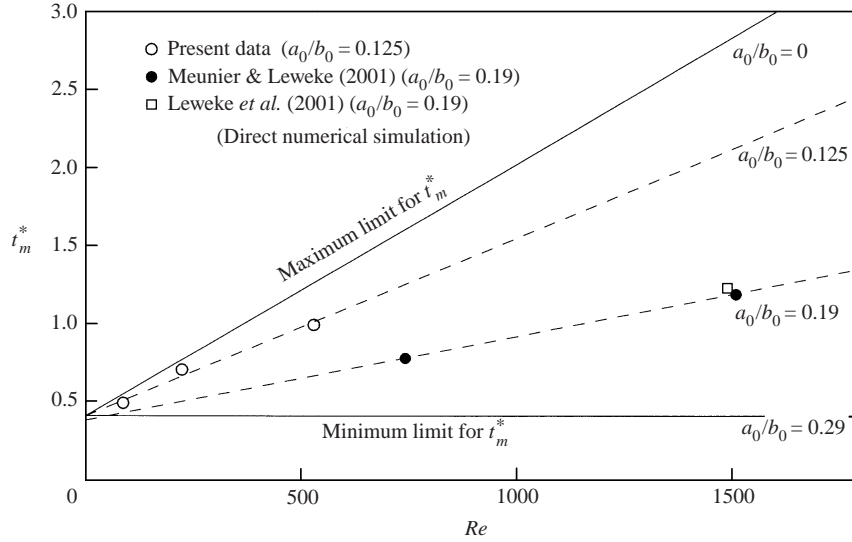


FIGURE 8. Normalized total merging time for laminar vortices, as a function of Reynolds number and the initial core size (a_0). The parameter t_m^* roughly represents the number of turns of the two vortices around each other, until complete merger occurs.

Although the convective period t_C is not dependent upon the viscosity, our measure of the core size $a(t)$ does indeed grow by diffusion during the convective stage, which is noticeable at these low Re . The core size is measured (as a function of time) in figure 5(c). At the end of merging, the core size (a_{end}), for all the Reynolds numbers, appears to follow the same line (the upper dashed line in figure 5c), which represents the function

$$\left(\frac{a}{b_0}\right)^2 = 2\left(\frac{a_{crit}}{b_0}\right)^2 + \text{const} \times (\tau - \tau_0), \quad (4.11)$$

where $\tau = tv/b_0^2$. Approximately, the vortex core area doubles during merging (to give the factor 2 above), as indicated also in Meunier & Leweke (2001), but at these low Reynolds numbers, the convective stage is long enough to allow significant diffusion of the vortex cores by the end of merging. The core radius at the end of merging (a_{end}) is thus given for laminar vortices roughly as

$$a_{end}^2 = 2a_{crit}^2 + \text{const} \times (vt_C) \quad (4.12)$$

and from the data in figure 5, we find roughly

$$\left(\frac{a_{end}}{b_0}\right)^2 = \frac{24.5}{Re} + 0.17. \quad (4.13)$$

In this section we have been concerned with laminar vortices, and we shall briefly discuss the time of merging for vortices which become turbulent during their initial formation in the next section.

4.2. Turbulent vortex merging

When the Reynolds numbers exceed about 800 in these experiments, turbulence forms in the wake of the wing span, and is wound up into the vortices during vortex roll-up. (Dosanjh, Gasperek & Eskinazi 1962, at comparable Reynolds numbers, also

	Re	α
Present data	1665	0.006
Dosanjh <i>et al.</i> (1962)	2000	0.005
Newman (1959)	20000	0.002
McCormick <i>et al.</i> (1968)	$\sim 10^6$	0.00005
Rose & Dee (1965)	$\sim 10^7$	0.0001

TABLE 2. Values of the Squire parameter (α) as a function of Reynolds number (Re). The values of the Squire parameters were computed from the original data of previous studies by Govindaraju & Saffman (1971).

found their wing-tip vortices to become turbulent shortly after roll-up.) The rapid decrease of vortex separation $b(t)$, for these turbulent vortices in the convective stage, is plotted in figures 9(a) and 9(b). However, the collapsed data that ensue, for all the Reynolds numbers, if one uses the non-dimensional timescale in figure 9(c), yields a larger normalized convective period than was found for the laminar vortices (equation (4.5)), as given below:

$$t_C = 16.1 \left(\frac{b_0^2}{\Gamma_0} \right). \quad (4.14)$$

The larger normalized convective time for turbulent vortices is due to changes in the strength of the vorticity responsible for pushing the two vortices together, and is discussed briefly in §5. (One should mention that the data in figure 9(c) has a slight downwards bend, indicating that the ‘merging rate’ does not follow the linear variation found for the laminar vortex merging in figure 7.)

Previous studies of turbulent vortices, at comparable Reynolds numbers ($Re \approx 2000$), by Dosanjh *et al.* (1962) showed that the vortex core size grew by turbulent diffusion, at a rate much higher than could be attributed to viscous diffusion, as might be expected. On the assumption that there was a Gaussian vorticity distribution, they deduced the following values of an eddy viscosity (ν_T): $\nu_T = 8\nu-10\nu$. Squire (1965) proposed a representation of the turbulent vortex as having a uniform eddy viscosity (ν_T), which is proportional to the circulation Γ , based on dimensional reasoning: $\nu_T = \alpha\Gamma$. The parameter, α , is now known as the Squire parameter, and several values from various studies were tabulated by Govindaraju & Saffman (1971) and are included in table 2. In the present case, for $Re = 1665$, we see a similar rapid growth in core size in figure 10(a), and if we also assume a Gaussian vorticity distribution, then we may deduce that $\nu_T \approx 9.7\nu$ (or $\alpha = 0.006$) in our case, which is in reasonable accordance with previous works (as in table 2). The turbulent vortex core $a(t)$ grows, as discussed in the review paper of Spalart (1998), as follows:

$$a(t) = \text{const} \times \sqrt{\nu_T(t + t_0)}. \quad (4.15)$$

A similar simple analysis to that for laminar vortices used in equation (4.9) yields, for turbulent vortices,

$$t_m^* = \frac{\text{const}}{\alpha} \left[\left(\frac{a_{crit}}{b_0} \right)^2 - \left(\frac{a_0}{b_0} \right)^2 \right] + 0.81. \quad (4.16)$$

The Squire parameter decreases only slowly with Reynolds number, suggesting a gradual increase in t_m^* with Reynolds number. From the variation of α as a function

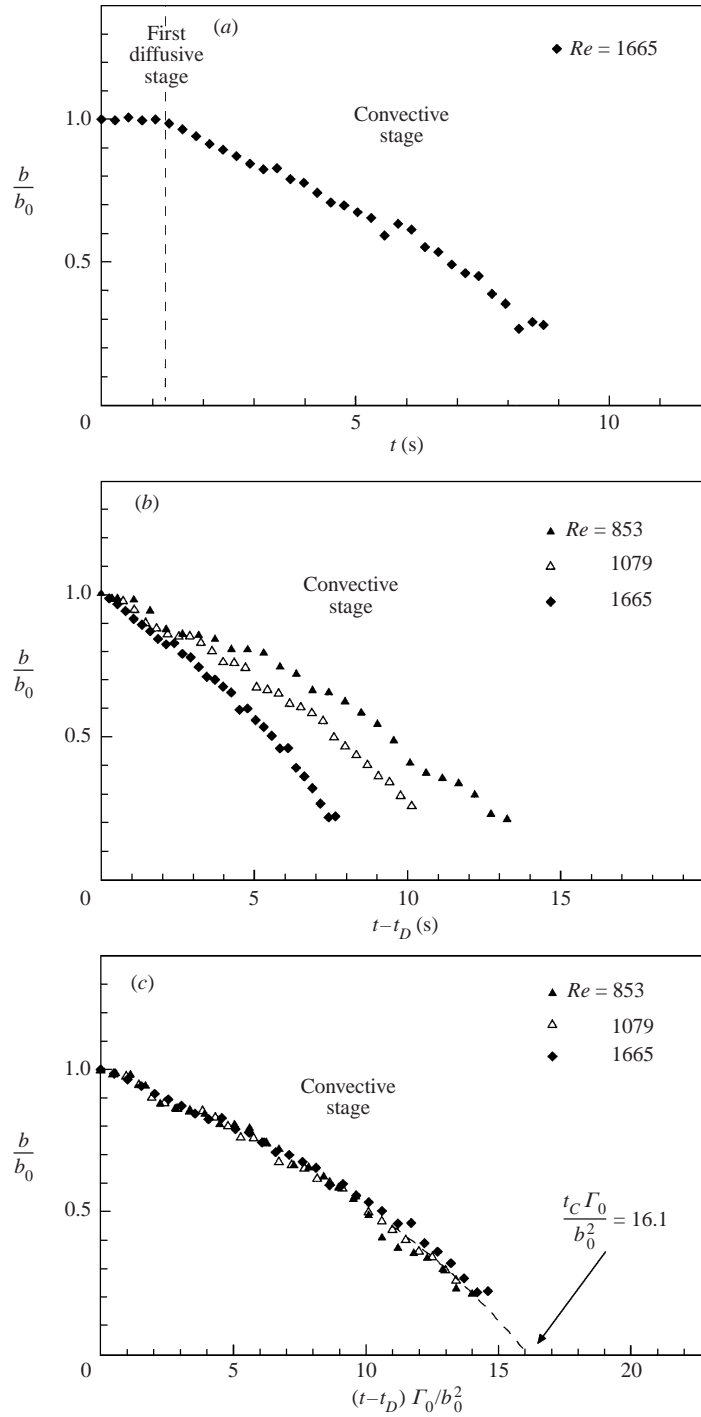


FIGURE 9. Evolution of the vortex separation distance versus time for turbulent vortex merger. The evolution of b/b_0 in (a) versus time shows the presence of a short *first diffusive stage*. Curves for different Reynolds numbers in the *convective stage* from (b), when plotted versus the non-dimensional convective time $(t-t_D)\Gamma_0/b_0^2$ in (c), collapse onto a single line.

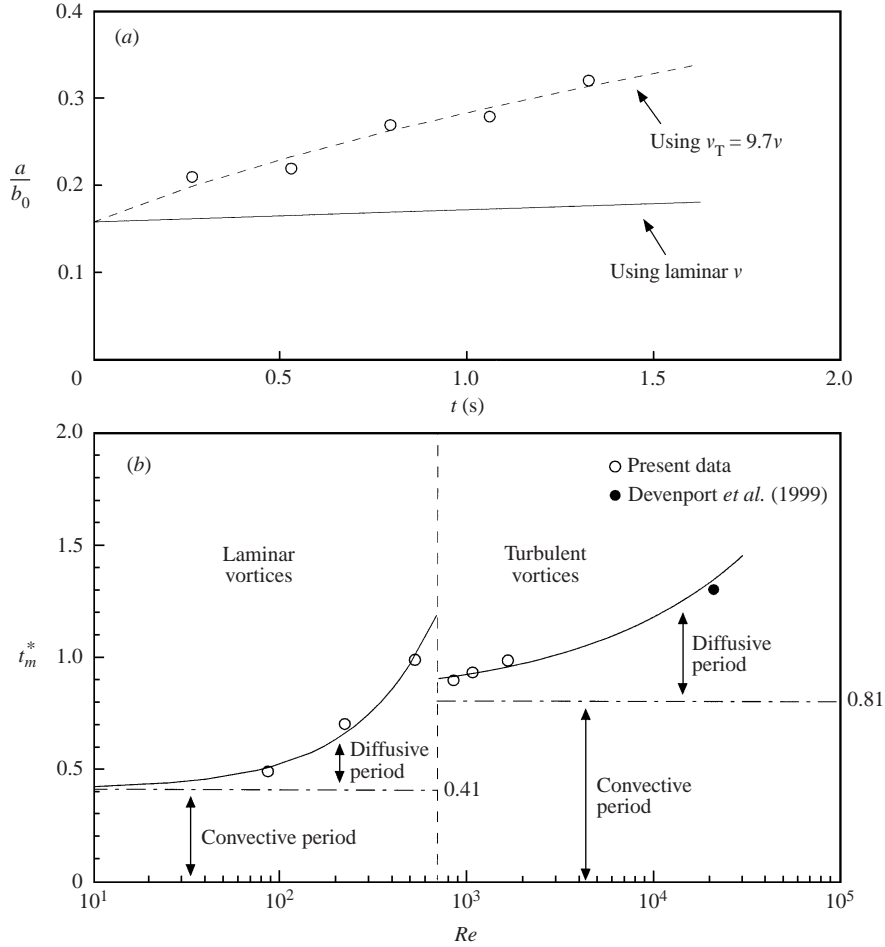


FIGURE 10. (a) The evolution of the vortex core size for $Re = 1665$. The vortex growth is faster than in laminar diffusion, and is well represented by using an effective turbulent viscosity $\nu_T \approx 9.7\nu$. (b) The non-dimensional merging time as a function of the Reynolds number, for laminar and turbulent merger.

of Re (a reasonable fit is given by $\alpha = 0.237/\sqrt{Re}$), one can formulate a rather approximate measure of the normalized merging time (t_m^*) as

$$t_m^* \approx 0.004\sqrt{Re} + 0.81. \quad (4.17)$$

The first term of this equation, which is the diffusive period (t_D^*), is not generally applicable for a range of turbulent vortices, because it depends on the vortex formation process (i.e. on initial size a_0). Nevertheless, the data point from the turbulent vortex study of Devenport *et al.* (1999) agrees reasonably well with equation (4.17), as plotted in figure 10(b). In general, one might suggest that the number of turns for complete merging of turbulent vortices (N) can be expected to be larger than the convective period found here, so that

$$N > 0.81, \quad (4.18)$$

which is supported by the data of Devenport *et al.* (1999) and by most of the range of data found in Chen *et al.* (1999) for $Re = 10\,000$ – $64\,000$.

In summary, for turbulent vortices, the convective period of merging is greater than for laminar vortices, but the diffusive period may be expected to be less, due to the rapid growth of core size under the action of turbulent diffusion.

5. Physical mechanism for vortex merging

In this section, we study the physical features of the flow that give rise to vortex merging. We demonstrate the advection of vorticity with reference to streamlines in a co-rotating reference frame. By decomposing the vorticity field into symmetric and antisymmetric components, we will see how the vorticity field causes the co-rotating vortices to be pushed towards each other, thus to merge into a single structure.

5.1. Streamlines in fixed and rotating reference frames

In order to clearly illustrate the essential difference between co-rotating vortices in a fixed reference frame, and in a rotating reference frame (rotating with the pair), we have computed the streamlines in both reference frames for a pair of point vortices, as shown in figure 11. The streamfunction in the fixed frame (on the left) is characterized by an internal regime encircling the vortex cores, and an external region where the fluid moves around the two vortices in an anticlockwise sense (similarly to the vortices themselves); the separatrices in figure 11 mark the boundary between the two regions.

One of the keys to understanding vortex merger is the use of a co-rotating reference frame, and we show the streamlines, as well as the separatrices on the right-hand side of figure 11. Instead of one type of region inside the closed separatrices, we now have three, and one notes that the flow external to this set of separatrices rotates in a clockwise sense (opposite to the vortex core rotation). In figure 12, we show only the principal regions of the flow, by extracting only the separatrices of the co-rotating streamline pattern. Here we define: an *inner core region*; an *inner recirculation region*, where fluid can travel around both vortices; and an *outer recirculation region*, where the fluid rotation is opposite to the rotation within the cores. Such streamlines have been computed in earlier studies for inviscid vortices by Dritschel (1985) and by Melander *et al.* (1988). (Melander *et al.* refer to these regions as the ‘compound core region’, the ‘exchange band’, and the ‘ghost vortex’. Dritschel had similar terminology, namely the ‘vortex region’, the ‘band region’ and the ‘umbrella region’). In this work, we choose a different nomenclature since we want to stress the distinction between the inner region and the outer region, because the separatrix between these areas is crucial to the physical mechanism of merging. In their inviscid computations, Melander *et al.* recognized the importance of streamlines to merging.

In previous studies, streamlines in a co-rotating reference frame have been shown only from two-dimensional inviscid computations. In figure 13, we show, for the first time, such streamlines from an experimental (and thus viscous) flow, where we may observe how the diffusing vorticity gradually changes the shape and topology of the streamline pattern. We place the two vortex centres on the horizontal axis, in the sequence of streamline patterns in figure 13. Experimental streamlines in figure 13(a) are typical of the topology found for the first diffusive stage, and may be compared with the typical previous computations of the idealized flow fields. As vortices deform and get pushed together in the convective stage in figure 13(b), the size of the separatrix regions somewhat diminishes, but it can be seen that the topology of the ‘inner region’ changes – there is only an ‘inner recirculation region’, without the ‘inner core’ region. The central saddle point vanishes, despite the fact that the vorticity still has two distinct peaks and merger is not complete at this point. In figure 13(c),

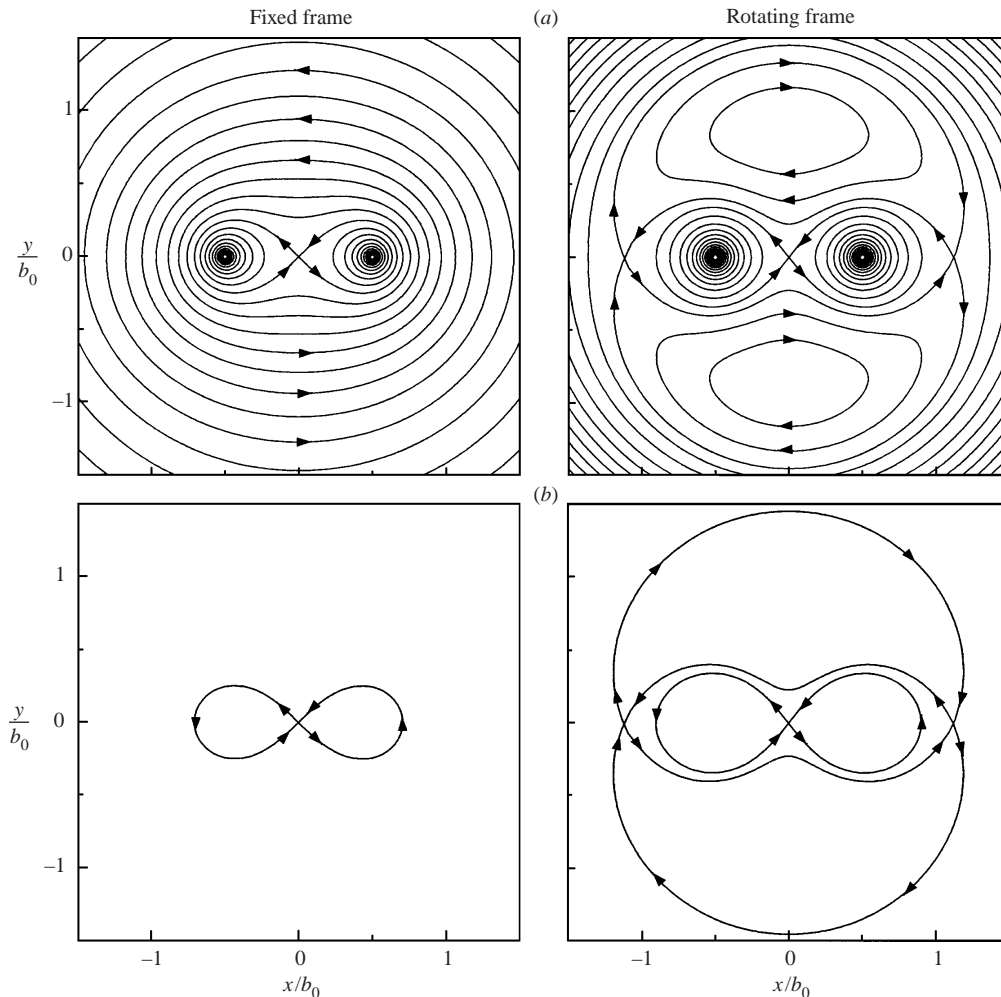


FIGURE 11. Patterns of (a) streamlines and (b) their separatrices in a fixed reference frame (on the left) and a rotating reference frame (on the right), for a pair of point vortices.

the vortices have merged and we shall see later that the larger inner region is able to capture some of the vorticity that had earlier diffused into the outer region, and this process of symmetrization (rather than axisymmetrization) is discussed further in § 5.5.

The juxtaposition between the vorticity and the streamlines is one of the key points to understanding the physics of merging (as recognized by Melander *et al.* 1987, 1988), and we now superpose the vorticity with the separatrices in figure 14. (We should note that for these figures, we have made the vorticity and streamlines skewsymmetric). In the first diffusive stage in figure 14(a), the two vortices have grown to the extent that they begin to diffuse non-negligible vorticity across the inner-outer separatrix (marking the boundary between the inner and the outer regions). One can see that vorticity diffused into the upper recirculation region will be advected by the flow field over to the left, whereas vorticity in the lower region is advected to the right. The next stage in figure 14(b) shows that the vortices start to deform and vortex filaments are formed, upwards to the left and downwards on the right. Later in the convective stage

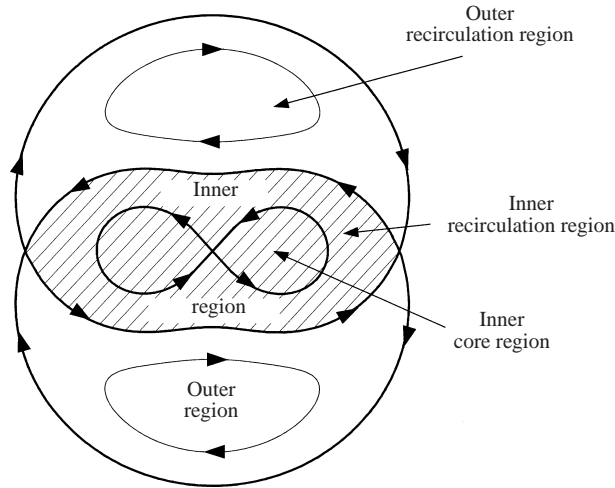


FIGURE 12. Diagram defining the regions of the flowfield bounded by separatrices of the co-rotating stream function.

in figure 14(c), the deformation is significant, and large asymmetric filaments have been generated. During this process, the vortex centres (peaks of vorticity) are pushed together, and this is clearly seen by comparing the deep red contours of figures 14(b) and 14(c).

In the inviscid computations of Melander *et al.* (1988), they expected that if vorticity is somehow placed in the ‘ghost vortex’ region (the outer recirculation region), it would ultimately cause filamentation, and then lead to merger. In these experiments, it is the viscous (or turbulent) diffusion which places the vorticity in the outer recirculating region that leads to the formation of filaments, after which merging is observed. We shall explain the physical mechanism for merging by considering the effect of the vorticity distribution on the induced velocity of the vortex centres, in the next section.

5.2. Physical mechanism for convective merging

It is straightforward to see that the formation of filaments will encourage the two vortex centres to move towards each other. If we take for example the upper left filament in figure 14(c), which comprises anticlockwise vorticity, one can imagine that its effect upon the left vortex centre is an induced velocity to the right. The vortex centre thus moves towards the other vortex, and the same reasoning holds for the other half of the flow. Filaments cause the vortex centres to approach each other, and merging ensues.

Melander *et al.* (1987) in their study of the axisymmetrization of ellipses, recognized that filaments represent asymmetric vorticity, and contribute to merging by their ‘axisymmetrization principle’. This principle showed that if elliptical-shaped vorticity contours are oriented at some angle (in their definition it needed to be a positive angle) with respect to the approximately elliptic streamlines, then a net velocity field ensued whereby the aspect ratio of the ellipse would be reduced. Melander *et al.* (1988) suggested that ‘merger is an inviscid axisymmetrization process’, similar to the single ellipse case. It will be possible to discuss this point, in the context of the present results, later.

In the present approach, we seek to formally decompose the complete vorticity field into symmetric and antisymmetric components. The vorticity and streamlines of

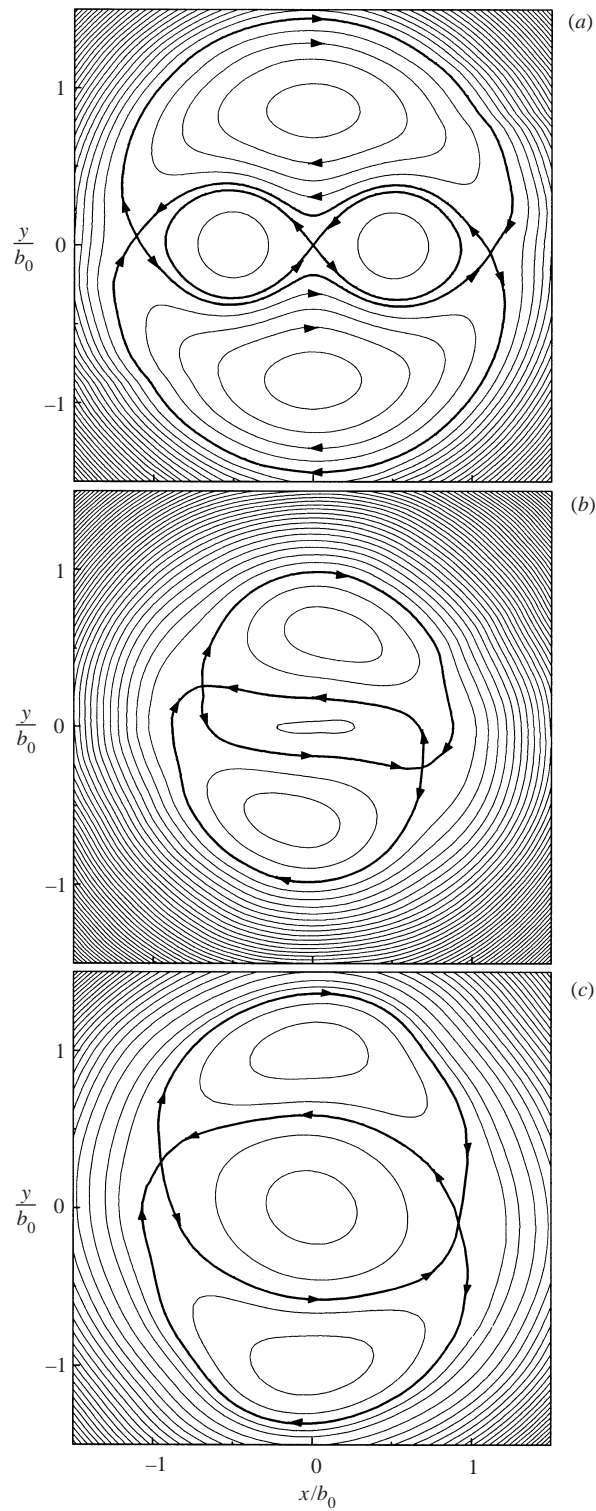


FIGURE 13. Experimental streamline pattern in a co-rotating reference frame during (a) the *first diffusive stage* ($t = 9.8$ s), (b) the *convective stage* ($t = 23.8$ s) and (c) the *merged diffusive stage* ($t = 37.1$ s). $Re = 530$.

figure 14, discussed earlier, were made skewsymmetric (symmetric about the origin):

$$\omega(x, y) = \omega(-x, -y). \quad (5.1)$$

Although this makes only a small difference to the vorticity field (with a maximum difference of less than 5% of peak vorticity), it helps to clarify our determination of the symmetric and antisymmetric vorticity in our presentation. The total vorticity $\omega(x, y)$ can be expanded as

$$\omega(x, y) = \frac{1}{2}[\omega(x, y) + \omega(x, -y)] + \frac{1}{2}[\omega(x, y) - \omega(x, -y)], \quad (5.2)$$

where the first term is the symmetric vorticity (ω_S) and the second term is the antisymmetric vorticity (ω_A):

$$\omega(x, y) = \omega_S(x, y) + \omega_A(x, y), \quad (5.3)$$

and where equations (5.1) and (5.2) ensure that

$$\omega_S(x, y) = \omega_S(-x, y) = \omega_S(x, -y), \quad (5.4)$$

$$\omega_A(x, y) = -\omega_A(-x, y) = -\omega_A(x, -y), \quad (5.5)$$

which are the conditions of symmetry and antisymmetry. We can now determine the symmetric vorticity by averaging the right half-plane of the total vorticity, in figure 15(a), with the left half-plane, resulting in the vorticity field of figure 15(b).

A comparison of the total velocity field (open arrows) with the velocity due only to symmetric vorticity (solid arrows) shows almost no difference, unless one zooms into the centre of the flow field, which we have done in figure 16. Clearly, the total velocity field has a component of velocity pushing the vortex centres (the bull's eyes) together, whereas the velocity from the symmetric vorticity has no such component. In fact, by inspection of the symmetric vorticity (in figure 15) one can deduce straightforwardly from the symmetry of the flow field that, along the x -axis, there is no component of horizontal velocity:

$$u_S(x, 0) = 0. \quad (5.6)$$

Therefore, it is solely the antisymmetric vorticity that is responsible for the approach of the vortex centres towards each other, so we are motivated to determine precisely the form of this vorticity for the complete flow field.

The antisymmetric vorticity, which we computed from equation (5.3), is now shown in figure 17. Immediately, one can see that this vorticity field comprises essentially two counter-rotating vortex pairs, whose induced velocity field and streamfunction (shown in figure 18) explain, rather clearly, why co-rotating vortices are pushed together during merger. In fact, the flow field is similar to a vortex pair in proximity to a vertical wall, although one cannot decouple this antisymmetric vorticity from the rest of the flow, except at a given instant of time.

We illustrate the flow field briefly using a point-vortex configuration as in figure 17(b). According to this particular configuration, the rate at which the co-rotating vortices (the bull's eyes in this figure) approach each other is given by the velocity induced at those vortex centres:

$$\frac{db}{dt} = \frac{2\Gamma_A b_A}{\pi(b_A^2 + h^2)} - \frac{2\Gamma_A b_A}{\pi[b_A^2 + (h + b)^2]}. \quad (5.7)$$

During the merging process in our case, we find that, rather approximately, $h^2 \ll b_A^2$

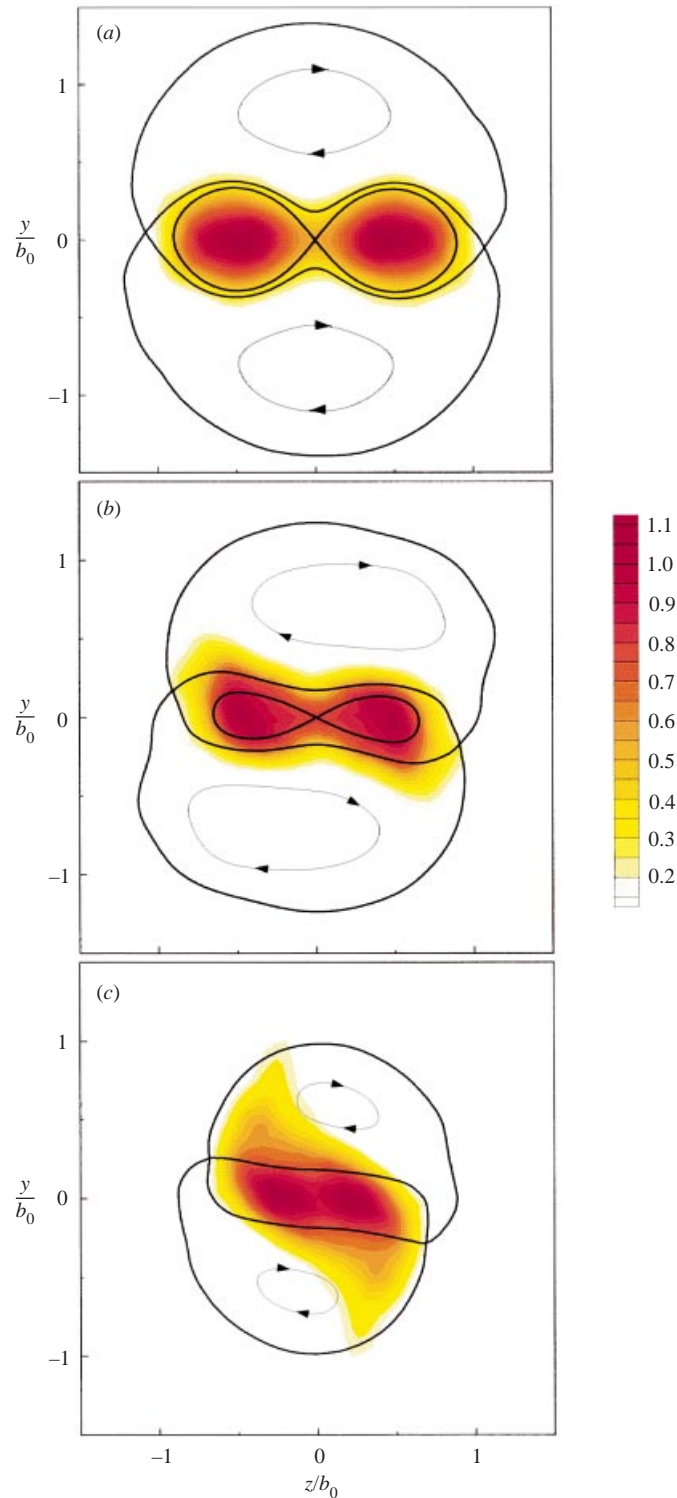


FIGURE 14. Vorticity field for a pair of co-rotating vortices superimposed on the separatrices of the co-rotating stream function, for the following stages: (a) the *first diffusive stage*; (b) at the end of the *first diffusive stage*; (c) the *convective stage*. $Re = 530$. In (a) $t = 9.8$ s, in (b) $t = 16.1$ s; and in (c) $t = 23.8$ s. Vorticity is counterclockwise. For these figures, we have made the vorticity and streamlines skewsymmetric.

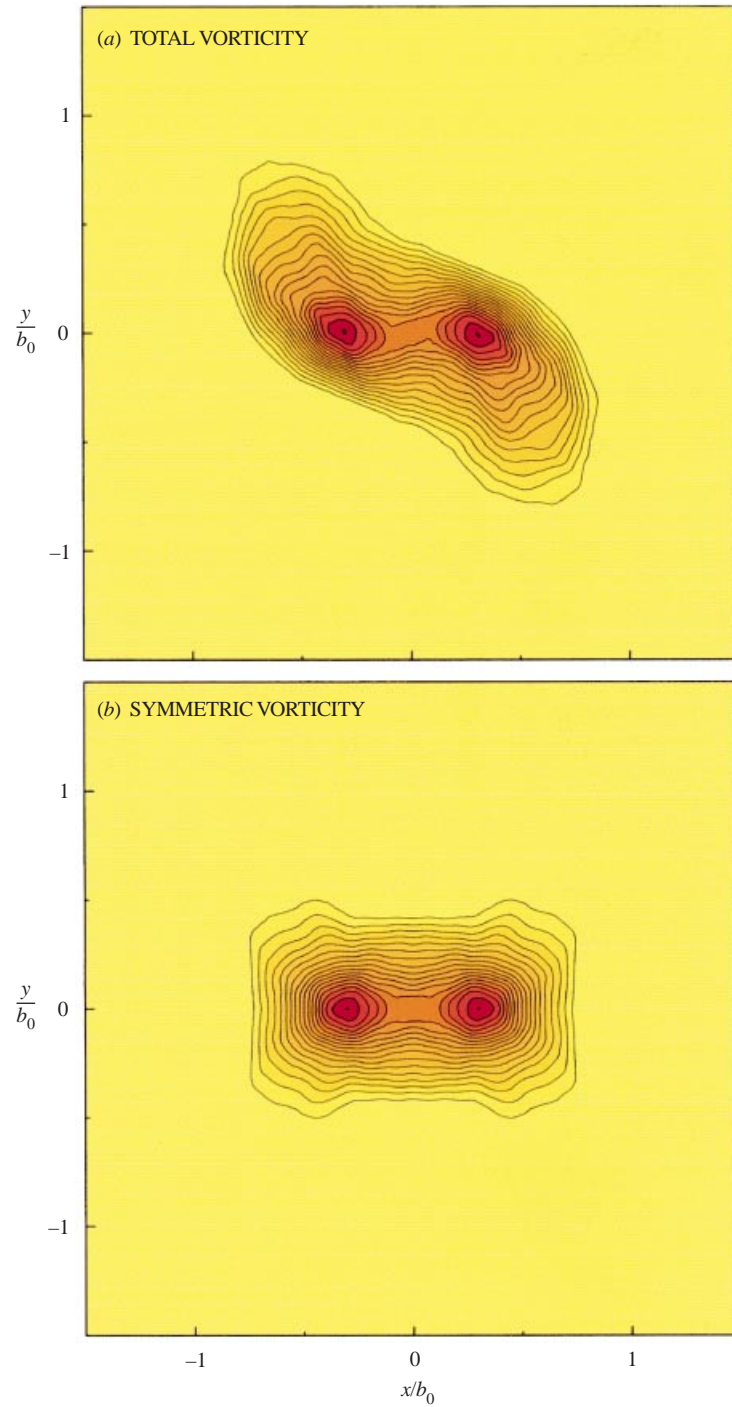


FIGURE 15. (a) Total vorticity field and (b) symmetric vorticity field during the convective merging stage. $Re = 530$, $t = 20.3$ s. Vorticity contours levels are $\omega = 0.15, 0.20, \dots$ (in s^{-1}). Vorticity is counterclockwise.

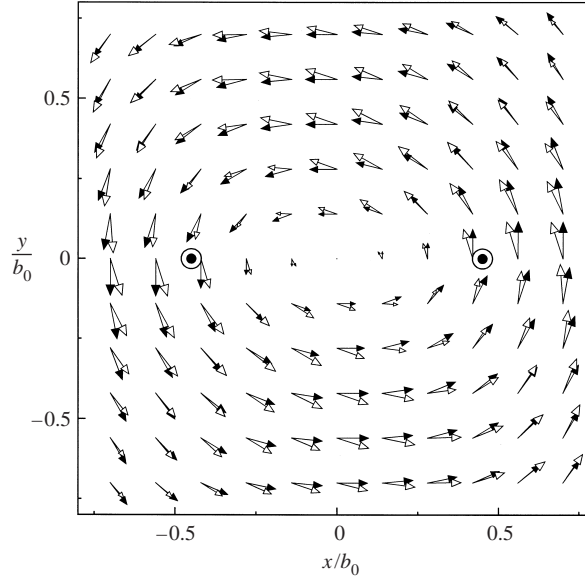


FIGURE 16. Total velocity field (open arrowheads) and symmetric velocity field (solid arrowheads). $Re = 530$, $t = 20.3$ s. The bull's eyes indicate the locations of the co-rotating vortex centres.

and $b_A^2 \ll b^2$, to give

$$\frac{db}{dt} \approx \text{const} \times \frac{\Gamma_A}{b_A}. \quad (5.8)$$

During the main part of the convective stage, we find that the strength of the antisymmetric circulation (Γ_A) is reasonably constant (see figure 20*b*) and so also is the height b_A , so that very roughly

$$\frac{db}{dt} \approx \text{const}, \quad (5.9)$$

which corresponds to the approximately linear decrease of $b(t)$ during convective merging in figure 4, and shown also in figure 19*b*.

We can measure the horizontal velocity of the vortex centres using the velocity field due to the antisymmetric vorticity (as typified by figure 17), and thus compute the 'merging velocity', db/dt during convective merging in figure 19*a*). We can also compute db/dt from the gradient of $b(t)$ in figure 19*b*). These methods to compute the merging velocity compare very well (as one should expect).

It should be said that for larger Reynolds number the antisymmetric vorticity flow field should still readily push together the vortex centres during merger, although one expects that the form of such vorticity will be different. The vortex filaments will be longer and wind around the perimeter of the outer recirculation region further than shown in our example here, leading to more elongated vortices when the antisymmetric vorticity is computed.

Before the start of convective merging, a certain amount of antisymmetric circulation (Γ_A) accumulates; therefore one expects a corresponding decrease in symmetric circulation (Γ_S), and these variations are shown in figure 20. An interesting feature concerning these plots, aside from the fact that Γ_A remains roughly constant over most of the convective stage, is that towards the end of merging, the antisymmetric circulation diminishes while the symmetric circulation correspondingly increases. This

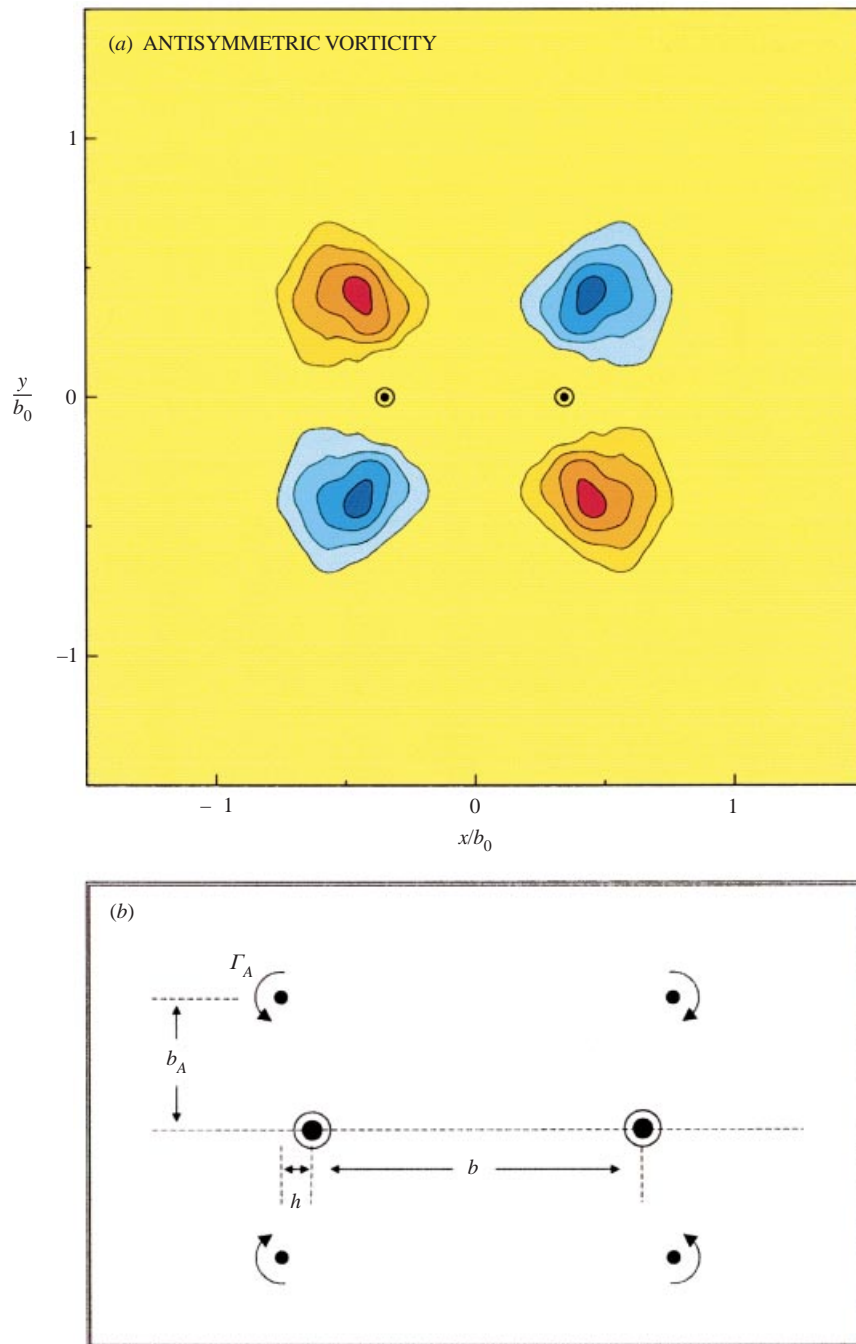


FIGURE 17. (a) Antisymmetric vorticity field, comprising two counter-rotating vortex pairs, whose induced velocity readily pushes the centres of the co-rotating vortices (the bull's eyes) towards each other. Vorticity contour levels are $\omega = \pm 0.15, \pm 0.20, \dots$ (in s^{-1}). Red vorticity is counterclockwise, blue vorticity is clockwise. $Re = 530$, $t = 20.3$ s. (b) Illustration of the antisymmetric flow field using a point-vortex representation.

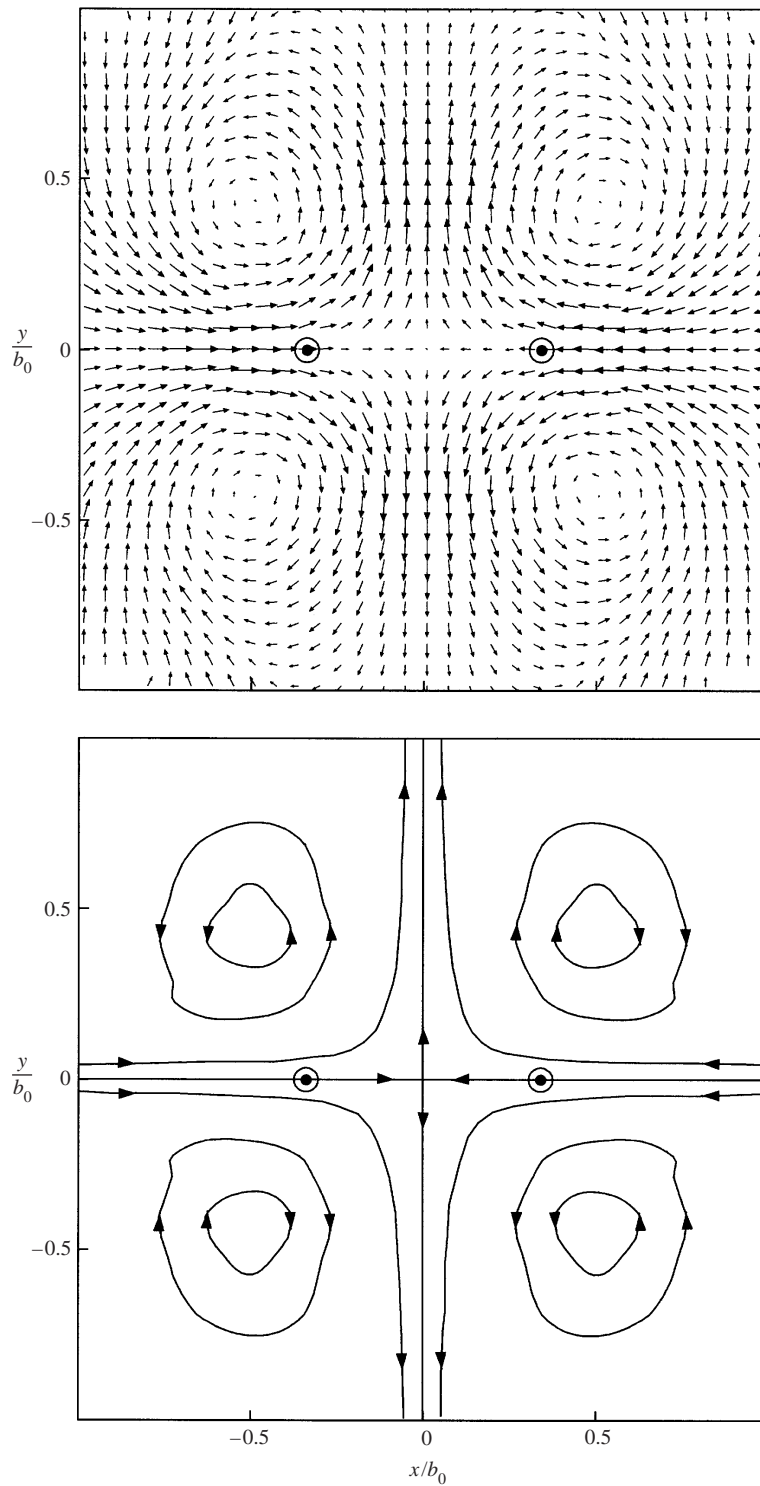


FIGURE 18. Velocity field and streamlines due to the antisymmetric vorticity, demonstrating clearly the counter-rotating pairs of vortices. Each half of the instantaneous flow field is equivalent to a vortex pair in proximity to a vertical wall. $Re = 530$, $t = 20.3$ s.

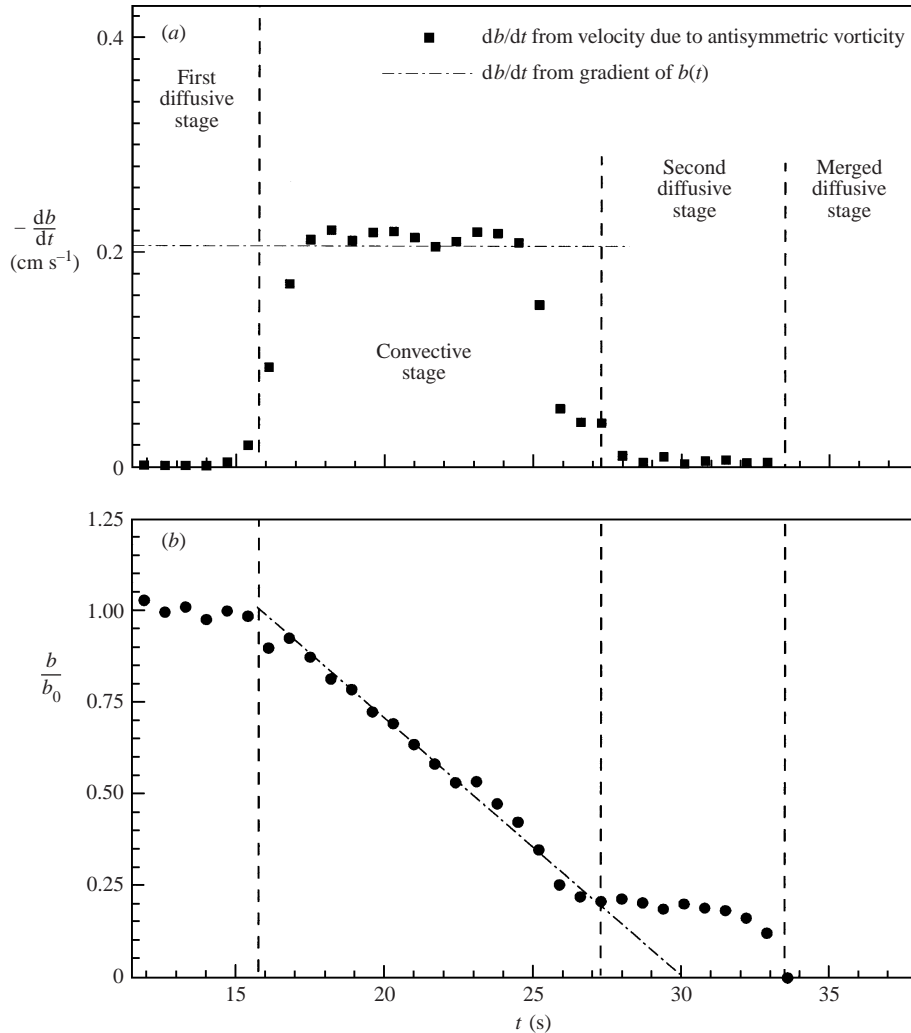


FIGURE 19. (a) Comparison of merging velocity (db/dt) measured from the velocity field due to antisymmetric vorticity (square symbols), and measured from the slope of the curve $b(t)$ in the convective stage (horizontal dash-dot line), showing good agreement. (b) The variation of $b(t)$ in the second diffusive stage, while the induced velocity in (a) is small. $Re = 530$.

process of *symmetrization* (we use this terminology as distinct from *axisymmetrization*) is further discussed in § 5.5.

5.3. Critical conditions for the inception of merging

It is now clear that for merger, we require a non-negligible diffusion of vorticity across the separatrix bounding the inner and outer regions. In our experimental flow, the vortices diffuse, due to viscous or turbulent effects, and place circulation into the outer region (Γ_{out}), which is subsequently advected by the flow field to generate antisymmetric circulation (Γ_A). An instructive measure of ‘outer circulation’ (Γ_{out}) can be computed from the simple flow field comprising two superposed Lamb–Oseen vortices, which is a reasonable approximation for the present experimental flow in the early stages of merging. The amount of outer circulation (Γ_{out}) is plotted versus

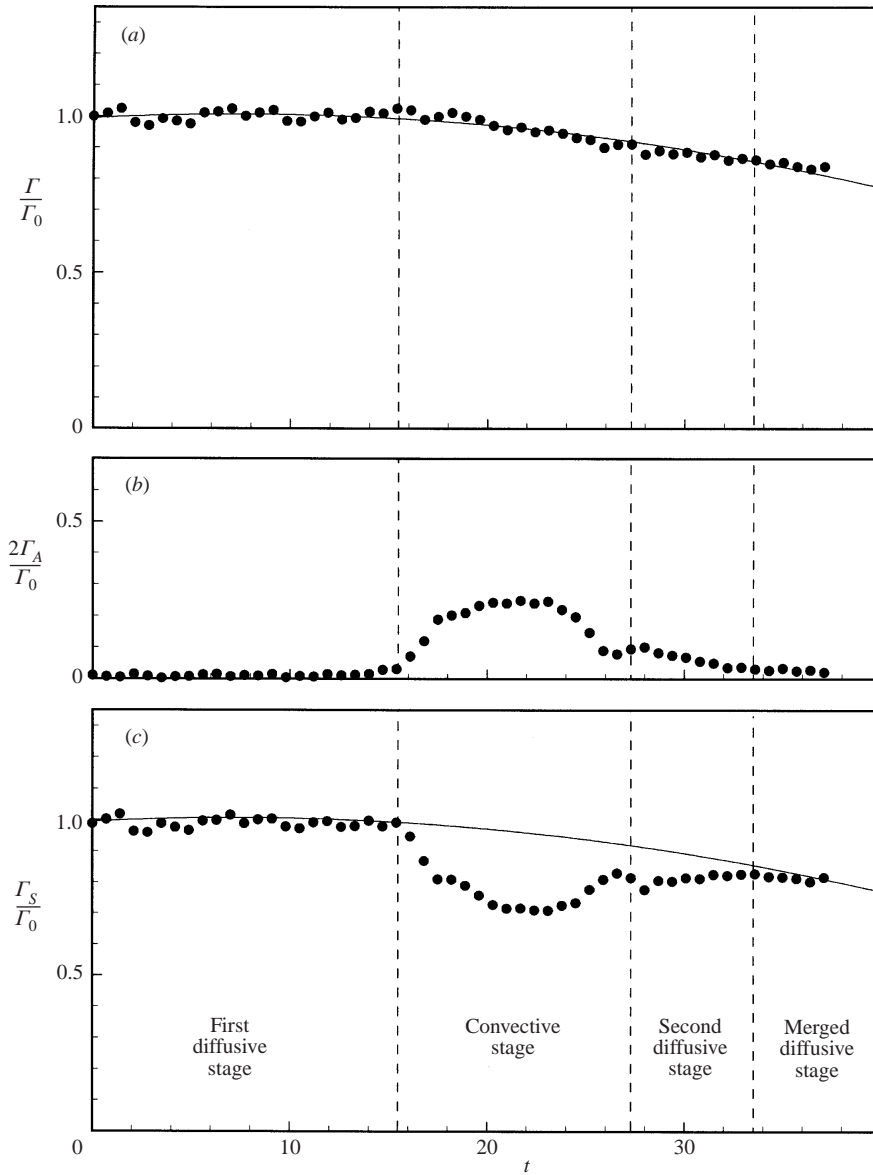


FIGURE 20. Evolution of the total circulation (Γ), the antisymmetric circulation (Γ_A) and the symmetric circulation (Γ_S) of the vortex pair. $Re = 530$.

the normalized core size of the vortices (a/b_0) in figure 21(a), and shows that we have non-negligible outer circulation (for example $\Gamma_{out} > 5\% \Gamma_0$) when $a/b_0 \approx 0.28$. Although clearly the choice of how much outer flow we should have to initiate merging is somewhat arbitrary, it is rather interesting that the Lamb–Oseen vortex representation predicts that non-negligible outer circulation will start to accumulate for about the same value of core size ($a/b_0 \approx 0.28$) as is found from the many computational, analytical and experimental studies mentioned in the Introduction, namely $a_{crit}/b_0 \approx 0.29\text{--}0.31$.

One expects that the accumulation of antisymmetric circulation, Γ_A (see figure 21b) will be delayed relative to the generation of the outer circulation (Γ_{out}), since it

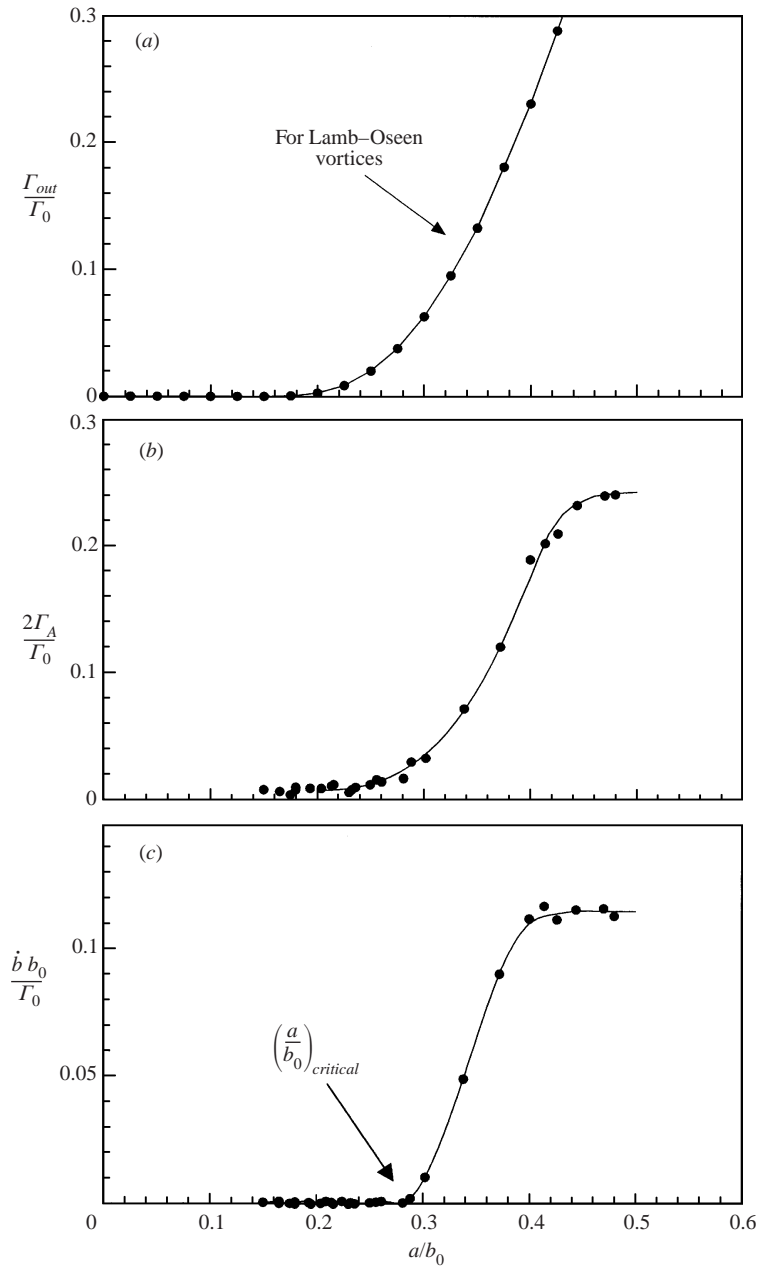


FIGURE 21. (a) The circulation diffused into the outer recirculation region for a pair of superposed co-rotating Lamb–Oseen vortices. (b) The antisymmetric circulation and (c) the normalized merging velocity $(db/dt)b_0/\Gamma_0$ for our experimental data ($Re = 530$). Significant movement of the vortices towards each other begins when approximately 3% of the total circulation becomes antisymmetric. The critical core radius is $(a/b_0)_{crit} = 0.29$.

takes some period of time for the outer vorticity to be advected, and then to become antisymmetric vorticity. In fact, throughout the convective merging stage, the antisymmetric circulation will always be less than the total outer circulation.

The superposed Lamb–Oseen vortex model (which can only be viewed as a rough approximation of the real flow) indicates well when one might expect merging to

commence. However, an indication of the critical conditions for the inception of merging is given by the variation of merging velocity, \dot{b} , in figure 21(c), which is of course dependent on the amount of Γ_A in (b). The curves appear to be well related to each other in figure 21. From (c), we may suggest a critical core size of

$$\left(\frac{a_{crit}}{b_0}\right) \approx 0.290 \pm 0.005, \quad (5.10)$$

which compares very well with core size value from Meunier & Leweke (2001), and is close to the theoretical values quoted in the Introduction. As the merging velocity starts to visibly increase, the corresponding critical antisymmetric circulation is around $(2\Gamma_A/\Gamma_0) \approx 3\%$. The antisymmetric circulation (Γ_A) and merging velocity (\dot{b}) both saturate at $(2\Gamma_A/\Gamma_0) \approx 24\%$, and $(\dot{b}b_0/\Gamma_0) \approx 0.12$, during the main part of the convective merging stage.

Some differences should be pointed out, at this point, between laminar and turbulent vortex merger. In the case of merging between turbulent vortices, the saturation level of the antisymmetric circulation only reaches the value $2\Gamma_A \approx 13\%\Gamma_0$, possibly due to a reorientation of primary vorticity as a result of three-dimensional instabilities and turbulence. This reduction of Γ_A causes the longer convective period found for turbulent vortices ($t_C\Gamma_0/b_0^2 = 16.1$) found in figure 9, which we mentioned in §4.

5.4. Second diffusive stage of merger

As vortices merge, there is a decrease in the vortex separation $b(t)$, as shown in figure 19(b). However, an interesting feature of this curve is the abruptly slower decay of $b(t)$ after $t = 27$ s. Such a bump or ‘tail’ in the curve of $b(t)$ was also observed in the computations of Leweke *et al.* (2001), and they mentioned that it is due to the persistence of two very low maxima (of vorticity) in the nearly formed vortex, which is not resolved in the corresponding experiments of that same paper. We note that in figure 19(a), the corresponding merging velocity (db/dt) has diminished almost to zero, as the induced velocity from the weak antisymmetric vorticity (the counter-rotating vortex pairs) becomes very small, especially as the vortex centres approach the centre of the hyperbolic flow field of figure 18. Thus, the induced velocity field is not sufficient to push the vortex centres completely together. So how does $b(t)$ ultimately become zero?

In order to answer this question, we again utilize (simply for illustrative purposes) the simple model of the superposed Lamb–Oseen vortices in figure 22. In this case, we place vortices at $x/b_0 = \pm 1/2$, and then allow them to diffuse (as though the vortices are independent of one another), but not actually to move towards each other. The vorticity diffusion in fact shifts the peak-vorticity locations towards each other, at first only slowly, as shown in figure 22(a), but then increasingly rapidly, until finally we have only a single peak in (b). The separation of vorticity peaks as a function of time for these Lamb–Oseen vortices is plotted in figure 22(c), where one can see the similarities with the experimental data. We note that our algorithm to find $b(t)$ simply finds the separation of the locations of peak vorticity. We conclude that the final reduction of vortex separation $b(t)$ to zero is not achieved through the induced velocities of antisymmetric vorticity (as for the convective stage) but represents instead the action of diffusion of vorticity. The vortices themselves are still separated by around $0.2b_0$, even after the fully merged condition is reached. Thus the initial shape of the merged vortex is elliptic rather than circular. The

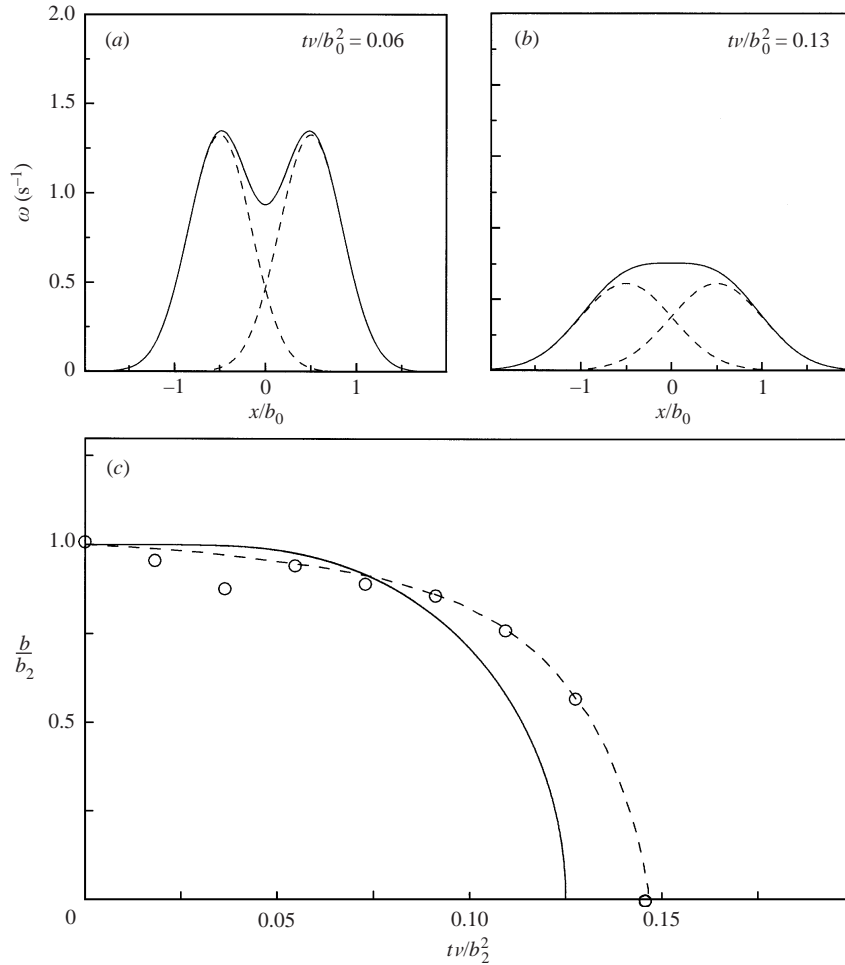


FIGURE 22. The *second diffusive stage*. (a,b) The evolution of the vorticity profile (through the line joining vortex centres) for a pair of co-rotating Lamb–Oseen vortices which have a constant vortex separation. (c) The evolution of the separation distance $b(t)$ between vorticity peaks for the Lamb–Oseen vortices (solid line) compares well with our experimental data for the second diffusive stage.

process described in this section represents a *second diffusive stage* in the dynamics of co-rotating vortices.

5.5. A symmetrization process during vortex merger

An interesting phenomenon occurs towards the end of convective merging, as indicated by figure 20. The antisymmetric circulation (Γ_A) diminishes, while the symmetric circulation (Γ_S) correspondingly increases. There is a ‘return to symmetry’, which can be understood by observing the development of the vorticity as it is advected by the instantaneous streamline patterns, in figure 23. The co-rotating streamfunctions are computed, taking into account the angular velocity of the vortex centres (or, ultimately, the elliptic merged vortex) as found in the plot of $\theta(t)$ of figure 5(a). We find that the growing inner region of the flow (bounded by the thicker line representing the separatrix) in figure 23(a,b) is able to ‘recapture’ vorticity that originally had escaped by diffusion into the outer region. Within the inner region, the vorticity recirculates

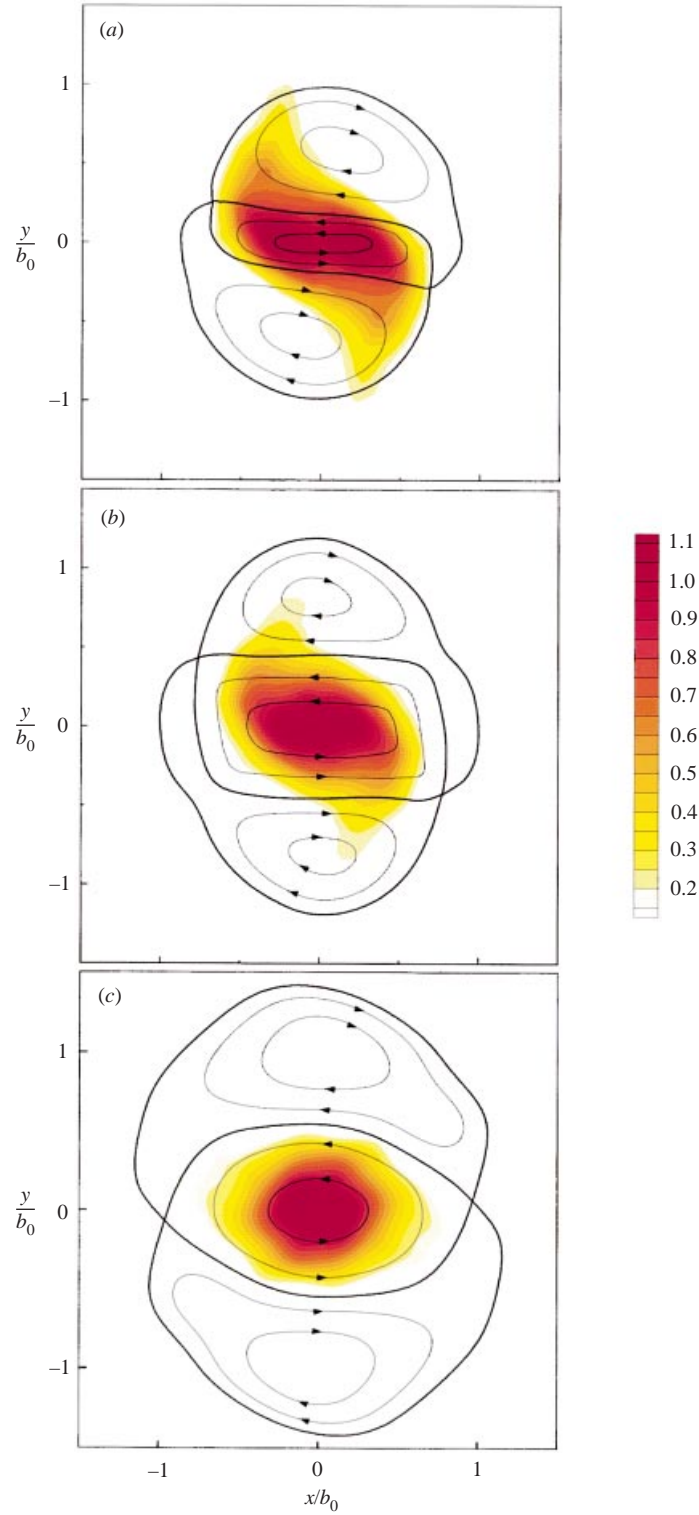


FIGURE 23. Vorticity field for a pair of co-rotating vortices superimposed upon the separatrices of the co-rotating streamfunction, during the symmetrization process. $Re = 530$: (a) $t = 23.8$; (b) $t = 25.2$; (c) $t = 32.9$. Vorticity is counterclockwise. The contour levels of vorticity are measured in s^{-1} . For these figures, we have made the vorticity and streamlines skewsymmetric.

in such a fashion that it returns to symmetry, as shown in figure 23(b,c); during this process, Γ_S increases as Γ_A decreases. This whole process represents a *symmetrization* of the vorticity field into an elliptical-shaped vortex.

6. Conclusions

In the present paper, we study the dynamics of co-rotating vortices, and their ultimate merger into one structure. There are four phases leading to vortex merging, namely a diffusive stage, a convective merging phase (when the vortex centres are rapidly pushed together), a brief second diffusive stage, and a final diffusion of the merged elliptic vortex. We have investigated the time periods for these different stages of co-rotating vortex interactions, and find that the initial stage is governed by diffusion (whether it be viscous or turbulent), while the period of the convective stage is scaled by the vortex circulation and the initial vortex separation, and is principally independent of diffusion. In the case of the laminar vortices, this corresponds well with the suggestions of Melander *et al.* (1988) regarding the scaling of the viscous and convective stages, and with the experimental results of Meunier & Leweke (2001). We find in this work a good collapse of data from experiments at different Reynolds numbers, yielding a convective period

$$t_C = 8.1 \left(\frac{b_0^2}{\Gamma_0} \right) \quad (6.1)$$

for laminar vortices, while the turbulent vortices convectively merge at a slower normalized rate: $t_C = 16.1(b_0^2/\Gamma_0)$. The total normalized merging time for laminar vortices is found to be

$$t_m^* = c_1 Re + 0.41, \quad (6.2)$$

where the first term represents the diffusive period, and the second term represents the convective merger period. The coefficient c_1 will vary between different situations, because it depends on the initial vortex core size, and this is dependent on the initial physical formation of the vortices. This normalized merger time t_m^* is approximately equal to the number of turns of the vortices around each other, before complete merger takes place. For turbulent vortices, the spread of the vortex core is governed by turbulent diffusion, and here we have used values of the Squire parameter from different vortex studies compiled by Govindaraju & Saffman (1971), to estimate the merger time as

$$t_m^* \approx 0.004\sqrt{Re} + 0.81. \quad (6.3)$$

The convective stage is, in essence, the ‘heart’ of the merging of two vortices, since, in this stage, the vortices rapidly move towards each other. If one observes the streamlines of this flow in a co-rotating reference frame, then one finds an inner and outer recirculation region of the flow, divided by a separatrix streamline. When the vortices grow large enough in the first stage, diffusion across the separatrix places vorticity into the outer recirculating region of the flow. This leads to the generation of asymmetric vorticity in the form of vortex filaments, and it is clear from considering the induced velocity from such filaments that these will push the co-rotating vortex centres together. In order to quantitatively analyse the merging process, we decompose the total vorticity into symmetric and antisymmetric components. Motivated by the fact that it is only the antisymmetric vorticity field which can give rise to merger, we directly measure the structure of this vorticity field. We discover that the form

of the antisymmetric vorticity comprises two counter-rotating vortex pairs, whose induced velocity field rather clearly pushes the two centroids together. The merging velocity, computed from the antisymmetric vorticity field, agrees closely with the merging velocity measured directly from the total (original) flow field, as one should expect. The start of the phase wherein the vortices approach each other is initiated approximately when the antisymmetric vorticity is around 3% of the total vorticity, and when the ratio between the vortex core radius and their separation is close to 0.29.

We believe that the physical mechanism of the merging process presented here is consistent with the ‘axisymmetrization principle’ of Melander *et al.* (1987, 1988) for elliptic vortices, which they believed would also hold for merging vortices. If one observes the pattern of the inner region of the co-rotating streamline pattern, it is indeed tilted with respect to the line joining the vortex cores (figure 14c). The considerations in Melander *et al.* suggest that this (positive) angle of orientation between streamlines and vorticity contours will yield a reduction of aspect ratio for the two-vortex system; one expects the vortices to move towards each other, thus to merge. Our mechanism is also consistent with the model discussed by Meunier (2001), who states that the increase in angular momentum due to the formation of filaments would correspond with a reduction of vortex separation distance, in order that the total angular momentum remains conserved.

During the late part of the convective merging stage, the antisymmetric vorticity is diminished by a *symmetrization* process, because the separatrix bounding the inner region of the flow becomes larger, and ‘recaptures’ some of the vorticity which originally escaped to become asymmetric vortex filaments. During this period, the induced velocity pushing vortex centroids together becomes too weak to cause the final merger into one structure. Final merging into one vorticity structure is achieved by a second diffusive stage, and in fact the original vortices are still separated by about 20% of their initial separation, when they become completely merged, yielding an elliptic merged vortex.

The support from the Ocean Engineering Division of ONR, monitored by Dr Tom Swean, is gratefully acknowledged (ONR Contract Numbers N00014-94-1-1197 and N00014-95-1-0332). The work of C. Cerretelli was also supported by the Rotary Foundation (Rotary International Ambassadorial Scholarship, 1998/99) and by the Gruppo Dirigenti FIAT (Borsa di Studio ‘Carlo Ghiglieno’, 1999/2000). We acknowledge with thanks the insightful comments of the reviewers and editor of this paper. We have benefited greatly from many discussions with Dr R. Govardhan, Dr S. Leibovich, Dr S. B. Pope, Ing. G. Nikitina and Dr C. Champagne. It has been especially fruitful and enjoyable to collaborate with Dr T. Leweke’s excellent research group at IRPHE, principally involving himself and Dr P. Meunier, to whom we owe a great deal of thanks!

REFERENCES

- ADRIAN, R. J. 1991 Particle imaging techniques for experimental fluid mechanics. *Annu. Rev. Fluid Mech.* **23**, 261–304.
- BRANDT, S. A. & IVERSEN, J. D. 1977 Merging of aircraft trailing vortices. *J. Aircraft* **14**, 1212–1220.
- BROWN, G. L. & ROSHKO, A. 1974 On density effects and large structure in turbulent mixing layers. *J. Fluid Mech.* **64**, 775–816.
- CHEN, A. L., JACOB, J. D. & SAVAS, O. 1999 Dynamics of corotating vortex pairs in the wakes of flapped airfoils. *J. Fluid Mech.* **382**, 155–193.

- CHRISTIANSEN, J. P. & ZABUSKY, N. J. 1973 Instability, coalescence and fission of finite-area vortex structures. *J. Fluid Mech.* **61**, 219–243.
- CLERCX, H. J. H., MAASSEN, S. R. & VAN HEIJST, G. J. F. 1999 Decaying two-dimensional turbulence in square containers with no-slip or stress-free boundaries. *Phys. Fluids* **11**, 611–626.
- COUDER, Y. 1983 Observation expérimentale de la turbulence bidimensionnelle dans un film liquide mince. *C. R. Acad. Sci. Paris II* **297**, 641–645.
- CROUCH, J. D. 1997 Instability and transient growth for two trailing-vortex pairs. *J. Fluid Mech.* **350**, 331–330.
- DEVENPORT, W. J., VOGEL, C. M. & ZSOLDOS, J. S. 1999 Flow structure produced by the interaction and merger of a pair of co-rotating wing-tip vortices. *J. Fluid Mech.* **394**, 357–377.
- DOSANJH, D. S., GASPAREK, E. P. & ESKINAZI, S. 1962 Decay of a viscous trailing vortex. *Aero. Q.* **13**, 167–188.
- DRITSCHEL, D. G. 1985 The stability and energetics of corotating uniform vortices. *J. Fluid Mech.* **157**, 95–134.
- DRITSCHEL, D. G. 1986 The nonlinear evolution of rotating configurations of uniform vorticity. *J. Fluid Mech.* **172**, 157–182.
- FREYMUTH, P. 1966 On transition in a separated boundary layer. *J. Fluid Mech.* **25**, 683–704.
- GOVINDARAJU, S. P. & SAFFMAN, P. G. 1971 Flow in a turbulent trailing vortex. *Phys. Fluids* **14**, 2074–2080.
- GRIFFITHS, R. W. & HOPFINGER, E. J. 1987 Coalescing of geostrophic vortices. *J. Fluid Mech.* **178**, 73–97.
- HOLMES, P., LUMLEY, J. L. & BERKOOZ, G. 1996 *Turbulence, Coherent Structures, Dynamical Systems and Symmetry*. Cambridge University Press.
- HOPFINGER, E. J. & VAN HEIJST, G. J. F. 1993 Vortices in rotating fluids. *Annu. Rev. Fluid Mech.* **25**, 241–289.
- HUERRE, P. & ROSSI, M. 1998 Hydrodynamic instability on open flows. In *Hydrodynamics and Nonlinear Instabilities* (ed. C. Godreche & P. Manneville). Cambridge University Press.
- JIMENEZ, J., MOFFATT, H. K. & VASCO, C. 1996 The structure of the vortices in freely decaying two-dimensional turbulence. *J. Fluid Mech.* **313**, 209–222.
- LE DIZES, S. & VERGA, A. 2002 Viscous interactions of two co-rotating vortices before merging. *J. Fluid Mech.* **467**, 389–410.
- LEE, J.-J. 1971 Wave-induced oscillations in harbours of arbitrary geometry. *J. Fluid Mech.* **45**, 375–394.
- LEWEKE, T., MEUNIER, P., LAPORTE, F. & DARRACQ, D. 2001 Controlled interaction of co-rotating vortices. *Aerospace Sci. Technol.* (submitted).
- LEWEKE, T. & WILLIAMSON, C. H. K. 1998 Cooperative elliptic instability of a vortex pair. *J. Fluid Mech.* **360**, 85–119.
- MCWILLIAMS, J. C. 1990 The vortices of two-dimensional turbulence. *J. Fluid Mech.* **219**, 361–385.
- MELANDER, M. V., MCWILLIAMS, J. C. & ZABUSKY, N. J. 1987 Axisymmetrization and vorticity-gradient intensification of an isolated vortex through filamentation. *J. Fluid Mech.* **178**, 137–159.
- MELANDER, M. V., ZABUSKY, N. J. & MCWILLIAMS, J. C. 1988 Symmetric vortex merger in two dimensions: causes and conditions. *J. Fluid Mech.* **195**, 305–340.
- MEUNIER, P. 2001 Etude expérimentale de deux tourbillons corotatifs. PhD thesis, Université de Provence Aix-Marseille I, France.
- MEUNIER, P. & LEWEKE, T. 2001 Three-dimensional instability during vortex merging. *Phys. Fluids* **13**, 2747–2750.
- MEUNIER, P. & LEWEKE, T. 2002 Elliptic instability of a co-rotating vortex pair. *J. Fluid Mech.* (submitted).
- MEUNIER, P., EHRENSTEIN, U., LEWEKE, T. & ROSSI, M. 2002 A merging criterion for two-dimensional co-rotating vortices. *Phys. Fluids* **14**, 2757–2766.
- OVERMAN, E. A. & ZABUSKY, N. J. 1982 A merging criterion for two-dimensional co-rotating vortices. *Phys. Fluids* **25**, 1297–1305.
- ROBERTS, K. V. & CHRISTIANSEN, J. P. 1972 Topics in computational fluid mechanics. *Comput. Phys. Commun.* **3**, 14.
- ROSSOW, V. J. 1977 Convective merging of vortex cores in lift-generated wakes. *J. Aircraft* **14**, 283–290.

- SAFFMAN, P. G. & SZETO, R. 1980 Equilibrium shapes of a pair of equal uniform vortices. *Phys. Fluids* **23**, 2339–2342.
- SPALART, P. R. 1998 Airplane trailing vortices. *Annu. Rev. Fluid Mech.* **30**, 107–138.
- SQUIRE, H. B. 1965 The growth of a vortex in turbulent flow. *Aero. Q.* **16**, 302–306.
- VINCENT, A. & MENEGUZZI, M. 1991 The spatial structure and statistical properties of homogeneous turbulence. *J. Fluid Mech.* **225**, 1–20.
- WESTERWEEL, J. 1993 *Digital Particle Image Velocimetry—Theory and Application*. Delft University Press.
- WILLERT, C. E. & GHARIB, M. 1991 Digital particle image velocimetry. *Exps. Fluids* **10**, 181–193.
- WINANT, C. D. & BROWAND, F. K. 1974 Vortex pairing: the mechanism of turbulent mixing layer growth at moderate Reynolds number. *J. Fluid Mech.* **63**, 237–255.
- ZABUSKY, N. J., HUGUES, M. H. & ROBERTS, K. V. 1979 Contour dynamics for the Euler equations in two dimensions. *J. Comput. Phys.* **30**, 96–106.